A 3D numerical model to Track Marine Plastic Debris (TrackMPD): Sensitivity of microplastic trajectories and fates to particle dynamical properties and physical processes

Isabel Jalón-Rojas, Xiao Hua Wang, Erick Fredj

A 3D numerical model to Track Marine Plastic Debris (TrackMPD): Sensitivity of microplastic trajectories and fates to particle dynamical properties and physical processes

Jalón-Rojas, I., Wang, X.H., Fredj, E.

DOI

https://doi.org/10.1016/j.marpolbul.2019.02.052

Publication date

2019

Document version

Accepted author manuscript

Published in

Marine Pollution Bulletin

Citation

Jalón-Rojas, I., Wang, X.H., Fredj, E. (2019). A 3D numerical model to Track Marine Plastic Debris (TrackMPD): Sensitivity of microplastic trajectories and fates to particle dynamical properties and physical processes, Marine Pollution Bulletin, 141, 256-272. doi: 10.1016/j.marpolbul.2019.02.052

A 3D numerical model to Track Marine Plastic Debris (TrackMPD): Sensitivity of microplastic trajectories and fates to particle dynamical properties and physical processes

Isabel Jalón-Rojas[1], Xiao Hua Wang[1,2] and Erick Fredj[3]

[1] The Sino-Australian Research Centre for Coastal Management, School of Science, UNSW Canberra, Canberra, Australia

[2] State Key Laboratory of Satellite Ocean Environment Dynamics (Second Institute of Oceanography, SOA), Hangzhou, China

[3] Jerusalem College of Technology, Jerusalem, Israel

Corresponding author: Isabel Jalón-Rojas (i.jalonrojas@unsw.edu.au; ijalonrojas@gmail.com)

Abstract

Numerical modelling is a key tool in understanding and determining the sources, trajectories and fates of micro-plastic debris (MPD). In this study, we introduce TrackMPD, a new modelling framework for the 3D transport of marine debris. TrackMPD fills the gaps in previous models by: (1) using a three-dimensional approach; (2) providing compatibility with a variety of ocean models; and (3) including a wide range of physical processes (advection, dispersion, windage, sinking, settling, beaching and re-floating) and MPD behaviours that depend on particle dynamical properties, and the fouling and degradation states. We implement a sensitivity analysis based on 44 scenarios to assess the relative importance of the different processes and behaviours on the MPD trajectories and fates. Results show that the MPD dynamical properties that impact their sinking, in particular plastic density and biofilm thickness and density, have the biggest effect on the MPD transport, followed by turbulent dispersion and washing-off.

Graphical abstract

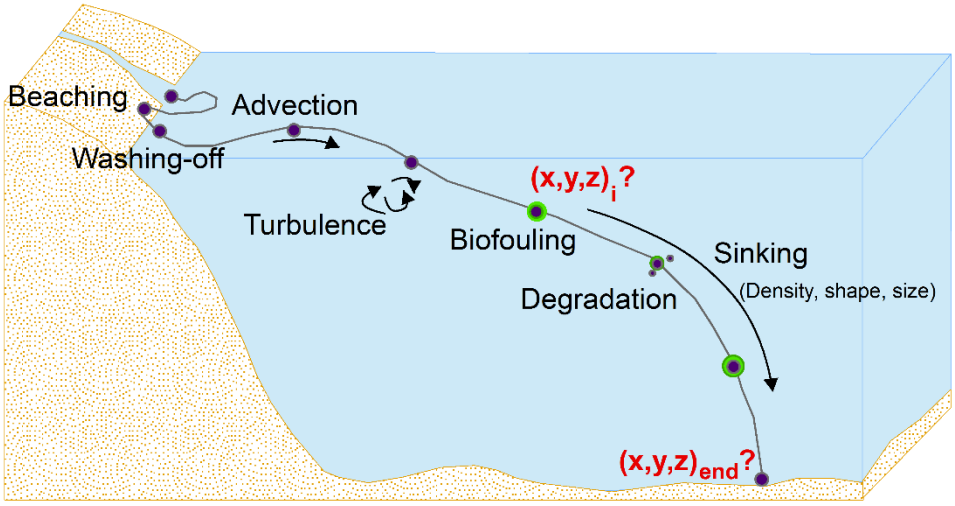

Keywords: Lagrangian tracking model; Marine plastic debris; Microplastics; Physical processes; Dynamical properties; Biofouling

Highlights

- Novel three-dimensional approach for modelling marine plastic debris transport
- Innovative modelling of physical processes and behaviour of microplastics
- High influence of vertical current shear on the dispersion of microplastics
- High impact of density and biofouling on sinking, and thus on trajectories and fates
- Particle size impacts the trajectories of spherical particles, but not of cylindrical

1. Introduction

Plastic pollution in marine regions is one of the most critical environmental issues affecting the world today. Global plastic production has dramatically increased over the last decades, up to 620% between 1975 and 2012 (*PlasticsEurope, 2013*), as did the amount of plastic waste entering the ocean. Plastic debris is now ubiquitous throughout marine systems in both surface waters and the sea bottom *(Ivar do Sul, 2007; Barnes et al., 2009; Eriksen et al., 2014, Ling et al., 2017*), while the incoming flux of plastic is expected to increase by an order of magnitude in the next decade (*Jamberk et al., 2015*). The growing spread of marine macro- (>5 mm) and micro- (<5 mm) plastic debris brings about a variety of ecological and socioeconomic risks, including physical damage of organisms (*Gregory, 2009*), habitat modifications (*Gall and Thompson, 2015*), the loss of ecosystem services (*Smith, 2012*) and the loss of tourism revenue (Jang et al., 2014). Microplastics can also enter and rise up the food chain, and be an effective vector for invasive species and chemical pollutants, harming biodiversity and human health (*Derraik, 2002*; *Browne et al., 2013*; *Clark et al., 2016*; *Koelmans et al., 2016*).

Increasing environmental concern about micro-plastic debris (MPD) has motivated numerous studies on its impacts, and there is a need for a better understanding of MPD behaviour, transport and fate (*Hidalgo-Ruz et al., 2012; Ivar do Sul and Costa, 2014*). Experimental research on MPD dynamic behaviour and numerical modelling are key approaches to progress in this field. Despite the former still being rare, recent studies have demonstrated the impact of physical properties of MPD on its motion. Plastic density, size and shape are the main properties governing the buoyancy and mobility of MPD (*Browne et al., 2010*; *Filella et al., 2015*, *Chubarenko et al., 2016*; *Zhang, 2017*). Higher densities and sizes decrease the buoyancy of MPD, which can affect its environmental distribution. This is shown by several in-situ surveys (*Hidalgo-Ruz et al., 2012; Enders et al., 2015*).

Quite recently, *Khatmullina and Isachenko* (*2017*) have made progress in parameterizing the impact of physical properties on MPD settling velocity by measuring the settling velocity of MPD of different densities, sizes and shapes, and comparing the values with existing semi-empirical formulations developed for natural sediments. This highlighted the most accurate formulations, and motivated the definition of a new formulation for cylindrical particles. MPD dynamic properties may be modified by fouling by organisms (so-called biofouling, *Barnes, 2002; Zettler et al., 2013*) and their incorporation in aggregates (*Long et al., 2015*). Biofouling increases the MPD specific density and size, contributing to a loss in buoyancy and an increase in settling velocity (*Morét-Ferguson et al., 2010; Hidalgo-Ruz et al., 2012; Chubarenko et al., 2016; Kaiser et al., 2017*). This may affect the MPD's final fate (*Rummel et al., 2017*). MPD may also become brittle over time as part of the degradation process, fragmenting into progressively smaller particles (*Weinstein et al., 2016; Jahnke et al., 2017*). There is evidence that the physical properties of MPD influence their buoyancy and motion, but the impact on the particles' final fate is still poorly understood.

Numerical models, in particular Lagrangian particle-tracking models coupled to ocean circulation models, are widely used to evaluate and predict potential MPD sources, pathways and fates under changing environmental conditions (see the compilation by *Liubartseva et al., 2016*). However, most of these models assume marine debris to be neutral particles drifting within the surface layers, omitting their dynamic behaviour and assuming a 2D approach (*Wakata and Sugimori, 1990; Isobe et al., 2009; Martinez et al., 2009; Kako et al., 2010; Yoon et al., 2010; Ebbesmeyer et al., 2012; Lebreton et al., 2012; Neumann, 2014; Mansui, 2015; Gajšt et al., 2016; Carlson et al., 2017; Liubartseva et al., 2018; Murray et al., 2018*). This may be attributed to the lack of parameterization, until recently, of MPD physical properties. The majority of MPD transport models thus not only ignore the sinking of particles, being only valid for neustic MPD, but also other physical and biological processes such as washing-off from the beach, bottom deposition, re-suspension from the bottom, fragmentation and biofouling (*Hardesty et al., 2017*; *Zhang, 2017*). Wind drift is usually included in numerical models tracking large macroplastics or objects (*Kako et al., 2010; Ebbesmeyer et al., 2012; Critchell and Lambrechts, 2016; Murray et al., 2018*). The omission of physical processes can in part be related to the fact that most studies on MPD transport focus on oceanic scales or in regional seas (review by *Liubartseva et al., 2016*) and ignore coastal processes. In addition, Lagrangian tracking models are typically inflexible, as they use hydrodynamic inputs from a specific ocean model (*Fredj et al., 2016*).

Despite these general features, some models have included improvements. *Liubartseva et al. (2018)* consider the sedimentation and washing-off of MPD using a Monte Carlo probability technique based on the particle age for sedimentation and the specific rate of washing-off and on the mean retention time on the beach for washing-off. The probability of sinking was considered to increase exponentially over time due to biofouling and interaction with sediments, but was independent of the particle properties. In addition, the vertical transport of particles, and therefore the different horizontal currents at different vertical layers, was taken into account. *Critchell and Lambrechts (2016)* also consider the MPD sinking and washing-off, but through temporal rates: beached particles washed-off into the sea surface layer and suspended particles settled on the bottom after a given time. Particle sinking was considered instantaneous and independent of biofouling and particle characteristics. *Iwasaki et al. (2017)* used a particle-tracking model that allowed particles to move vertically as a function of their size, but within a depth of 0–5 m. These studies used a 2D approach, and hence ignored the fact that the settling of particles together with vertical current shear can impact the MPD transport. The importance of vertical current shear in the transport of microplastics has indeed been demonstrated for low-density floating microplastics moving in a coastal bay under strong turbulence (Jalón-Rojas et al., 2019). Until now, the sinking velocities of particles in a 3D approach has only been considered in the MARBLE model (Bagaeve et al., 2017). Both MARBLE and the OceanParcels Lagrangian analysis toolkit (Lange and Van Sebille, 2017) track plastic particles in the flow field simulated by external hydrodynamic models. Notwithstanding these developments, MPD tracking models still need substantial improvement to better

represent the different dynamical behaviours of particles and the key physical processes, so as to improve their predictive capabilities.

The aim of this work is to develop and present TrackMPD, a new modelling framework for the 3D transport of marine plastic debris that incorporates the main physical processes relevant to plastic and MPD behaviours. Following recent experimental work (*Zhiyao et al., 2008*; *Chubarenko et al., 2016*; *Khatmullina and Isachenko, 2017*), TrackMPD includes the particle properties that define the MPD behaviour (density, size, shape), the processes affecting their variations (biofouling, degradation) and the parameterizations of physical processes (advection, diffusion, windage, sinking, beaching, washing-off, deposition). Based on the Particle Tracking and Analysis Toolbox (PaTATO, *Fredj et al., 2016*), TrackMPD is a user-friendly tool, compatible with velocity data from different sources. We implement the model for Jervis Bay and its adjacent coast (SE Australia) in order to illustrate application of the model and answer the following questions:

- to what extent is it important to model the transport of different types of MPD in three dimensions?

- how do physical processes and the physical properties of particles affect the transport and fate of MPD and what is their relative impact?

This paper is organized as follows. Model structure, equations and numerical solutions are provided in Section 2. Section 3 describes and discusses a sensitivity analysis to assess the relative influence of different processes and behaviour model parameters on MPD trajectories and fates, using Jervis Bay as a natural laboratory. Conclusions are drawn in Section 4.

2. The TrackMPD modelling framework v.1

TrackMPD is a three-dimensional non-Lagrangian particle-tracking model for the transport of marine plastic debris in oceans and coastal systems. The power of TrackMPD lies in: (1) its compatibility with diverse formats of current-velocity inputs; and (2) its ability to extend the Lagrangian modelling of advection-diffusion by adding more-complex and realistic particle behaviours and physical processes, which can either be included or excluded depending on the application. At present, TrackMPD can include windage, beaching, washing-off, degradation, biofouling, sinking and deposition. In particular, sinking and deposition depend on particle behaviour, which relies on the particle density, size, shape, fouling state and degradation state. The model can incorporate new processes and behaviours, and change the implementation of already existing ones, with new experimental findings or particular applications.

TrackMPD has thus a structured and coherent modelling framework to satisfy the criteria of flexibility, extendability and interchangeability. This framework is based on the Particle Tracking and Analysis

Toolbox (PaTATO, *Fredj et al., 2016*), which can already use velocity data from various sources, such as different ocean general circulation models (OGCM: e.g. POM, ROMS and MITgcm) and satellite observations, and can compute forward and backward trajectories in two or three dimensions. The model consists thus of a set of coupled and mutually interacting modules. Modules are independent functions or classes that define behaviours, read the inputs from a certain source, implement a given physical process or perform auxiliary tasks such as create outputs. This allows independent development of modules that can be easily added to the model without the need to change the other modules. Furthermore, TrackMPD is a user-friendly tool developed in Matlab, and therefore is easily accessible by a wide audience.

2.1. Modular structure

2.1.1. Input modules

As a first step, TrackMPD reads the input file (Fig. 1), in which users define the following information.

- **Hydrodynamic model name, domain, grid and parameters.** TrackMPD supports velocities defined in rectangular Arakawa A and C grids, and in depth (z) and sigma (σ) vertical coordinates. Version 1.x is compatible with a range of OGCM, such as POM, ROMS and MITgcm; this range will be extended in future versions.
- **Physical processes and behaviours.** Turbulence, behaviour, washing-off and windage modules can be turned on/off. Parameters of selected processes (Section 2.2) are defined at this step.
- **Trajectory setting.** The simulation period is defined by the time step, the trajectory duration, the trajectory direction (forward or backward) and the time of particles' release. The particle location is defined from a .cvs file which contains four columns: longitude; latitude; depth (in meters); and date of birth (the time in seconds from when the simulation starts until when the particle is released).

2.1.2. Trajectory computation module

The marine debris trajectories are calculated off-line, i.e. after the OGCM has been integrated and the velocity fields have been stored (Fig. 1). This makes it possible to calculate many more trajectories than with online calculation. The model has external and internal time steps, Δt_i and $\Delta t_{G,}$ respectively. Boundary-condition algorithms prevent particles from leaving the model domain and determine if a particle has beached or been deposited on the bottom. The external time step Δt_G is the time step of the OGCM model output (e.g. 30 min). The internal time step Δt_i is the time interval during which particle movement is calculated (e.g. 1 min). The internal time step is smaller than the external time step so that particles do not move in large jumps that could cause inconsistencies between the predictions of the

OGCM model and the particle-tracking model. At each internal timestep of TrackMPD, particle motion is calculated as the sum of movement due to advection, turbulence and behaviour. The model contains sub-models for each of these components (Fig. 1). The equations and solution methods used in these subroutines are detailed in Section 2.2.

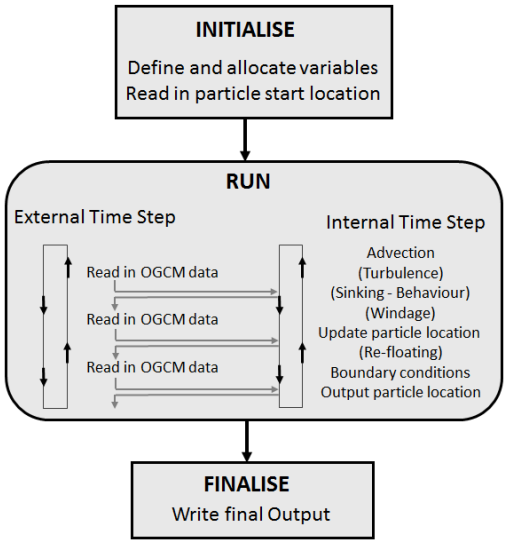

Fig. 1. Flow diagram of the TrackMPD transport model. Optional processes are indicated by brackets. Black arrows represent the external and internal loops. Grey arrows represent the data exchange between the external and internal loops.

2.1.3 Output module

TrackMPD allows users to select the output parameters, time step and format (Matlab or NetCDF). Output data can contain model results, such as particles trajectories and fate (position and type – water, seafloor or land), and the model setting and inputs. The NetCDF format allows the output visualization and postprocessing in a range of software packages.

2.2. Equations and solution methods

2.2.1. General equations

TrackMPD is established in a three-dimensional domain extending in the zonal (x), meridional (y) and vertical (z) directions. Advective, diffusive and sinking displacements determine the 3D trajectories of particles according to

$$dX(t) = dX_{adv}(t) + dX_{diff}(t) = U(x,y,z,t)dt + dX'(t) \quad (1)$$

$$dY(t) = dY_{adv}(t) + dY_{diff}(t) = V(x,y,z,t)dt + dY'(t) \quad (2)$$

$$dZ(t) = dZ_{adv}(t) + dZ_{diff}(t) + dZ_{sink}(t) = W(x,y,z,t)dt + dZ'(t) - w_s(t)dt. \quad (3)$$

The advective displacement $d\boldsymbol{X}_{\boldsymbol{adv}} = (dX_{adv}, dY_{adv}, dZ_{adv})$ is given by the Eulerian velocity field $\boldsymbol{U} = (U,V,W)$, which is provided by the OGCM, but can also include wind velocities. OGCM do not simulate turbulent motion at scales smaller than the grid resolution of the model. In particle-tracking models, particles can be moved in millimetre to centimetre steps — much less than the hydrodynamic model grid scale. A random component $d\boldsymbol{X}' = (dX', dY', dY')$ must be added to the particle motion to reproduce turbulent diffusion $d\boldsymbol{X}_{\boldsymbol{diff}} = (dX_{di}, dY_{diff}, dZ_{diff})$ that occurs at the scale of the particle motion. The sinking displacement dZ_{sink} depends on the settling velocity w_s. The model can also compute 2D trajectories from two-dimensional modelled or observed velocity fields $\boldsymbol{U} = (U,V)$ by ignoring the term $dZ(t)$.

2.2.2 Numerical solution

Interpolation scheme

It is necessary to interpolate in time as well as in space because the duration between successive outputs of the OGCM model is longer than the time step of the marine debris particle motion. OGCM model predictions are read in and interpolated in space and time to the particle location. The first step in the process of interpolating the water properties (e.g. current velocities, salinity, temperature, sea surface height, vertical and horizontal diffusivities) to the particle location is to determine the grid cell in which the particle is located. Once the particle is in a grid cell, water properties are interpolated in space to the particle location. All water properties are interpolated from the native OGCM grid points (e.g. *u*-grid points are used to calculate the *u*-velocity at the particle location, *v*-grid points are used for the *v*-velocity and rho grid points are used for sea surface height, *w*-velocity, salinity and diffusivity calculations). For three-dimensional water properties (e.g. current velocities, diffusivities, salinity), a water-column profile scheme is applied. In this scheme, values are interpolated along each *s*-level to create a vertical profile of values at the *xy* particle location.

Advection

A Runge-Kutta scheme of order 4/5 in both space and time is used to calculate particle movement due to advection (Eq. (4)). This scheme solves for the current velocities $\boldsymbol{U} = (U,V,W)$ at the particle location using an iterative process that incorporates velocities at previous and future times to provide the most robust estimate of the trajectory of particle motion in water bodies with complex fronts and eddy fields. Current velocities (m/s) provided by the Runge-Kutta scheme are multiplied by the duration of the internal time step Δt_i to calculate the displacement of the particle in each component direction.

Displacements (m) are then added to the original location of the particle (x_n,y_n,z_n) in order to calculate the new location of the particle (x_{n+1},y_{n+1},z_{n+1}):

$$\begin{aligned} x_{n+1} &= x_n + U\Delta t_i \\ y_{n+1} &= y_n + V\Delta t_i \\ z_{n+1} &= z_n + \mathrm{W}\Delta t_i \end{aligned} \qquad (4)$$

Turbulence

A random-walk model is used to simulate turbulent particle motion in the horizontal (x or y) directions. When the horizontal diffusivity K_h is constant, the random-displacement model defaults to a random-walk model:

$$x_{n+1} = x_n + R[2r^{-1}K_h\Delta t_i]^{1/2}\,, \qquad (5)$$

where K_h in m^2/s is evaluated at x_n. R is a random number with mean zero and standard deviation r =1. TrackMPD reproduces sub-grid-scale turbulent particle motion in the vertical (z) direction to mimic the debris turbulent particle motion in that direction:

$$z_{n+1} = z_n + R[2r^{-1}K_v\Delta t_i]^{1/2}\,, \qquad (6)$$

where z_n is the initial particle location and K_v is the vertical diffusivity.

Sinking and deposition

The settling velocity w_s (m/s) occurs when the net gravitational force (gravity minus buoyancy) equals the drag force. It is a characteristic feature of any negatively buoyant particle, and determines its sinking displacement:

$$z_{n+1} = z_n - w_s(t_i)\Delta t_i\,. \qquad (7)$$

w_s can be directly defined by users or calculated by TrackMPD according to the particle behaviour (physical properties, biofouling, degradation; see Section 2.2.3). In the last case, it can remain constant or vary over time under the influence of biofouling and degradation. Particles reaching the sea bottom are considered as settled particles.

Windage

Very low density objects may float, and so can be highly exposed to wind. TrackMPD allows users to include the direct drift of spherical and cylindrical objects caused by wind through the advection formulation Eq. (4). In that case, the velocity field $\boldsymbol{U}$ is given by current (U_c,V_c,W_c) and wind (U_w,V_w,) velocities (m/s) as follows:

$$U = \frac{U_c + U_w\sqrt{\frac{\rho_{air}}{\rho_{water}}\frac{S_{above}}{S_{below}}}}{1+\sqrt{\frac{\rho_{air}}{\rho_{water}}\frac{S_{above}}{S_{below}}}} \qquad V = \frac{V_c + V_w\sqrt{\frac{\rho_{air}}{\rho_{water}}\frac{S_{above}}{S_{below}}}}{1+\sqrt{\frac{\rho_{air}}{\rho_{water}}\frac{S_{above}}{S_{below}}}} \qquad (8)$$

where ρ_{air} and ρ_{water} are the air and water densities (g/cm^3), respectively, and S_{above}/S_{below} is the ratio between the dry and wet cross-sectional areas of the particles. This formulation comes from the balance between the wind pressure force acting on the upper part of the particle and the water drag force on the underwater part, ignoring viscous forces (*Anderson et al., 1998*). S_{above}/S_{below} is the result of the balance between gravity acting on the particle of density ρ and the Archimedean force h due to current pressure on the underwater part of the particle:

$$\left(\frac{h}{R}\right)^2 \cdot \left(3 - \frac{h}{R}\right) = 4\frac{\rho}{\rho_{water}}. \qquad (9)$$

S_{above}/S_{below} is calculated in TrackMPD following *Chubarenko et al. (2016)* from ρ (g/cm^3), ρ_{water} (g/cm^3) and the radius of the sphere or cylinder R (m):

$$\frac{S_{above}}{S_{below}} = \frac{2\pi}{(\alpha - \sin\alpha)} - 1, \qquad (10)$$

where $\alpha = 2\arccos(1 - h/R)$, with the ratio h/R the numerical solution of Eq. (9).

Beaching and washing-off

Marine debris can reach land and beach on the near-shore. Beached debris can be trapped on the coast or washed off on the next incoming tide (*Johnson, 1989; Johnson and Eiler, 1999; Hinata et al., 2017*). TrackMPD allows users to include a range of conditions to reproduce this behaviour. In particular, TrackMPD v.1 is able to read tidal elevation data and wash off debris at high tide. In addition, it includes a Monte Carlo approach with probability P of being washed off, based on Lagrangian oil-spill models (*Al-Rabeh et al., 2000*):

$$P = 0.5^{-t/T}, \qquad (11)$$

where t is the time step from the last beaching and T is the half-life for debris to remain on the beach before being washed off again. This approach assumes that the probability of washing-off decreases exponentially with time due to interaction with the coastline (*Liubarzeva et al., 2018*). Beached debris can be washed off from the coast to the sea at high tides to its last position before beaching if a randomly generated number (between 0 and 1) is less than P. TrackMPD will include more-complex formulation in future versions to better reproduce the washing-off by tides, and also by waves.

2.2.3. Behaviour parameterization

The sinking behaviour of simulated marine debris is determined by the settling velocity w_s (Eqs. (3) and (6)). This parameter can be a model input for any kind of marine debris, macro-plastics, MPD or any other kind of object. In the case of MPD, TrackMPD allows the temporal estimation of w_s according the MPD behaviour. MPD behaviour is defined by its physical properties (density, shape, size), which can change over time under the effect of biofouling or degradation. Settling-velocity estimation for different behaviours is described below. It is based on recent experimental research, and may be easily modified in future model versions as a result of new experimental findings or particular applications.

Physical properties

MPD behaviour mainly depends on three characteristics: density; shape; and size (*Ballent et al., 2012; Chubarenko et al., 2016; Khatmullina and Isachenko, 2017; Kooi et al., 2017*). The specific density of plastic particles depends on the type of polymer, ranging from <0.05 g/cm^3 for foamed polystyrene to 2.3 g/cm^3 for teflon (*Chubarenko et al., 2016*). Denser particles of the same size and shape settle sooner (*Kooi et al., 2017*). The size of MPD identified in the environment is very variable (*Cole, 2016*), with 5 mm widely recognized as the maximum size. Lower sizes vary between studies, and depend on the sampling method (i.e. mesh size of the net, typically from 3 to 5 mm; *Hidalgo-Ruz et al., 2012*). Particles of the same density but larger size increase the ratio of the gravitational force acting on the particle to the viscous resistance of the fluid, and therefore the settling velocity. Common shapes of MPD are fibers, pellets and fragments of various geometries, from spherical to irregular. Primary MPD (the result of direct release) usually have regular shapes (such as beads or spherules), whereas secondary MPD (exposed to degradation) show diverse shapes (*Khatmullina and Isachenko, 2017*). Old fragments are characterized by smooth edges due to the ongoing polishing by other particles or sediment (*Doyle et al., 2011*). Elongated shapes are associated with large particles, while small particles are usually more spherical (*Gilfillan et al., 2009*). The shape of MPD determines the nature of its motion, and therefore influences its settling velocity (*Isachenko et al., 2016*).

Despite the well-known impact of these physical properties on MPD settling velocity, only very few studies have been concerned with its parameterization. *Khatmullina and Isachenko* (*2017*) measured the settling velocity of around 600 microplastics of different sizes (from 0.5 to 5 mm) and shapes (spheres, short cylinders (diameter ≈ length) and long cylinders), and compared the observed values with several empirical predictions developed for natural sediments. There was reasonable agreement except for long cylinders, for which a new approximation was proposed. The *Zhiyao et al.* (*2008*) formulation provided one of the best fits to data without the need for calibration. TrackMPD can incorporate this type of formulation. In particular, TrackMPD v.1 uses the Zhiyao and the Katmullina and Isachenko formulations to calculate the settling velocity of spherical and cylindrical MPD, respectively, as a function of their density and size: radius R (m) for spheres; radius R (m) and length L (m) for cylinders:

Spheres (*Zhiyao et al., 2008*):

$$w_s = \frac{\upsilon}{2R} d_*^3 \left(38.1 + 0.93 d_*^{12/7}\right)^{-7/8}, \qquad (12)$$

where $d_* = 2R(g(\rho_{p-} \rho_w)/\rho_w \nu^2)^{1/3}$ is the dimensionless particle diameter, ρ_p the particle density, ρ_w the water density (same units as ρ_p), υ the water kinematic viscosity (m^2/s) and g the gravity acceleration (m/s^2). w_s is calculated in m/s.

Cylinders (*Katmullina and Isachinko, 2017*):

$$w_s = \frac{\pi}{2}\frac{1}{\upsilon} g \frac{(\rho_p - \rho_w)}{\rho_w} \frac{2RL}{55.238L + 12.691}. \qquad (13)$$

This formulation provides w_s in mm/s, and requires the previous transformation to mm of all the variables involving a longitudinal scale.

Both formulations can be used for short cylinders. Other shapes, such as films or flat angular particles, and other MPD characteristics, such as the surface texture, might be considered in future model versions in line with the development of experimental studies and semi-empirical formulations. The specific MPD density can be selected as a function of the polymer type from the compilation of densities by *Chubarenko et al. (2016)*, which has been included in the TrackMPD package.

Biofouling

The growth of algae, invertebrates, bacteria or microbes on particle surfaces, so-called biofouling, can increase the size and density of MPD, and therefore contribute to a loss of its buoyancy (*Loeb and Neihof, 1975; Zardus et al., 2008; Rummel et al., 2017*). Particles initially characterized by positive buoyancy can sink into the water column or even became incorporated into deep sediment layers on the sea bottom (*Thompson, 2004*). TrackMPD can include the impact of this process on MPD trajectories by increasing the size and density of fouled particles. Following simple geometrical rules proposed by *Chubarenko et al. (2016)*, the density ρ_p of a fouled particle due to a biofilm layer of thickness BT can be approximated by

Spheres:

$$\rho_p = \rho_0 \frac{R_0^3}{(R_0 + BT)^3} + \rho_D \left[1 - \frac{R_0^3}{(R_0 + BT)^3}\right], \qquad (14)$$

Cylinders:

$$\rho_p = \rho_0 \frac{R_0^2}{(R_0 + BT)^2} + \rho_D \left[1 - \frac{R_0^2}{(R_0 + BT)^2}\right], \qquad (15)$$

where R is the radius of the original particle, ρ_0 is the density of the polymer and ρ_f is the biofilm density.

In TrackMPD, the biofouling can be considered as either a stationary or non-stationary process. In the first case, the particle is characterized by a constant biofilm thickness (BT) over time, representing a given biofouling state. In non-stationary biofouling, the thickness can vary over time according to a range of formulations. Even if there is evidence of a progressive temporal increase in BT (*Ye and Andrady, 1991; Morét-Ferguson et al., 2010; Lobelle and Cunliffe, 2011*), to our knowledge, there are no experimentally based parameterizations of these processes. TrackMPD v.1 includes an increase in the biofilm thickness at a constant rate BR to give some insight into the impact of this non-stationary process on MPD trajectories:

$$BT = BT_0 + BR\,\Delta t, \qquad (16)$$

where BT_0 is the initial biofouling thickness and Δt is the time step. This assumption was made in previous studies to calculate the MPD sinking period (*Chubarenko et al., 2016*). More-accurate parameterizations will be included in future model versions in line with new experimental research.

Degradation

The degradation of plastic in the environment can be induced by light, heat, oxygen and organisms. Highly degraded plastics become brittle enough to fall apart in fragments (*Andrady, 2011*). This process usually takes a long time, 50 years or more for plastic to fully degrade (*Müller et al., 2001*). However, fragmentation may start early in the swash zone (*Efimova et al., 2018*) and in some coastal systems such as salt marshes (around 8 weeks according to *Weinstein et al., 2016*), and therefore can impact MPD transport at seasonal time scales. Specific models for MPD should be developed to help understand and properly predict this complex process. The aim of this study is not to develop this kind of model or an accurate parameterization of model degradation and fragmentation. However, we include a simple parameterization of the MPD size decrease over time to gain some insight into the relative impact of a progressive MPD wear on MPD trajectories. For this purpose, MPD size decreases at a constant rate DR, which affects the settling velocity:

$$\text{Size } (D \text{ or } L) = \text{Size}_0\,(1 - DR \bullet T/100), \qquad (17)$$

where Size_0 is the initial diameter D or length L of the particle and T is the time from the beginning of the degradation to the current time step. DR is the percentage of size decrease per day, which can be applied to different shapes. It is based on the quantification of the temporal evolution of MPD properties in some experimental research (*Weinstein et al., 2016*). This parameterization allows a preliminary assessment of the potential impact that degradation may have on MPD tracking. However,

a proper simulation of MPD degradation needs better formulation based on laboratory studies and field monitoring.

3. Application and sensitivity analysis

TrackMPD has been applied to a case study in Jervis Bay and its adjacent coast (SE Australia, Fig. 2a). Jervis Bay is a semi-enclosed embayment 15 km long and 8 km wide, with an average depth of 15 m (Fig. 2c). The aim of this application is to demonstrate the ways TrackMPD can be used to include different physical processes and MPD behaviours, and to discuss the relative impact of these physical processes and behaviours on the trajectories and fates of MPD. While there is evidence of the presence of MPD in Jervis Bay (*Ling et al., 2017*), evaluating potential trajectories and accumulation zones of MPD in this system is not the focus of this work. The proposed simulations use idealized values for the model parameters to assess the importance of the processes and behaviours represented and, ultimately, to demonstrate the importance of the three-dimensional tracking of MPD.

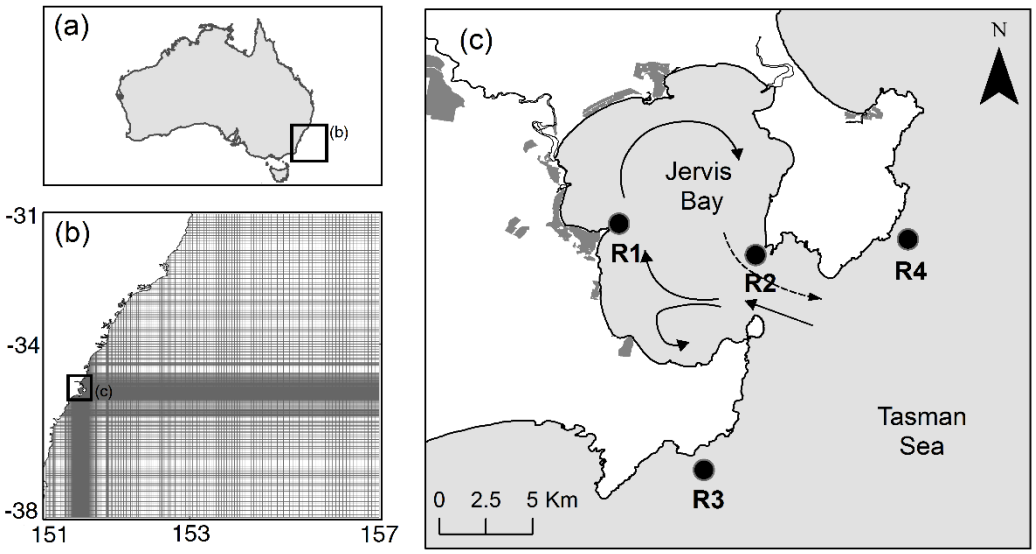

Fig. 2. Jervis Bay and its adjacent coast: **(a)** location map (SE Australia); **(b)** POM grid and domain; **(c)** the bay and the seeding locations for the sensitivity simulations (black circles). Shaded areas represent urban zones. Solid and dashed arrows represent the surface and bottom circulation patterns of the bay, respectively, during the simulation period.

3.1 Model settings

Jervis Bay has been the focus of numerous modelling studies to explain its hydrodynamic processes using the Princeton Ocean Model (POM; *Wang and Symonds, 1999; Wang, 2001; Sun et al., 2017; Liao and Wang, 2018*). POM is a sigma-coordinate, free-surface, primitive-equation ocean model, which includes a turbulence sub-model (*Mellor, 1998*). In this application, we use the POM hydrodynamic model results from 24 June to 11 July 1998 to force TrackMPD. This is the period used in the previous studies to validate POM in Jervis Bay, obtaining a very good fit to observations (see validation details

in *Sun et al., 2017*). The mesh size ranges from 500 m around the bay to 7 km at the open boundaries (Fig. 2b). Twenty-one sigma layers were considered vertically, with higher resolution near the surface and bottom. The model was forced by tides, heat flux, wind stress, daily mean temperature, salinity and currents. Hydrodynamic outputs (currents, salinity, temperature) were provided in 1-hour increments. During the simulation period, the bay was characterized by its typical circulation pattern; clockwise and anticlockwise circulations in the northern and southern basin, respectively. The flow exchange through the entrance was characterized by warm near-surface inflow on the southern side, and cold deeper outflow on the northern side (Fig. 2). Readers should refer to *Sun et al. (2017)* for more details on the hydrodynamic model setting.

A total of 44 sensitivity scenarios (Table 1, Supplementary Material A) were simulated to evaluate the relative importance of the physical processes (horizontal dispersion, vertical dispersion, washing-off and sinking) and behaviours (physical properties, biofouling and degradation) for MPD transport. The "control" scenario did not include any physical process or behaviour, except advection-dispersion with relatively small diffusivity coefficients — i.e. the microplastics were considered to be passive particles. Windage was not included in the sensitivity analysis since it is only relevant for the transport of floating objects (*Critchell and Lambrechts, 2015).*

Degradation occurs at long time scales (from several months to tens of years, *Weinstein et al., 2016*) so its relative influence cannot be compared with other faster processes. Therefore, we analysed the impact of degradation independently of the main sensitivity analysis. The degradation rates were overstated to provide an insight into the potential influence of this process. For biofouling, we compared the behaviour of particles with a constant biofouling state (given by the biofouling thickness and density) and particles subject to temporally varying biofouling (given by the biofouling rate). The biofouling rate has yet to be quantified, as explained in Section 2.2.3, so its real influence cannot be properly evaluated. However, we used some reasonable values following descriptive observations (e.g. biofouling visible after several days or weeks; *Ye and Andrade, 1991*; *Lobelle and Cunliffe, 2011*), in order to gain some insight into its influence on MPD transport. Model parameters for the different scenarios are given in Table 1. Where possible, they were values from the literature (key references are in Table 1). To analyse the sensitivity to model parameters, their values were changed one by one in the different scenarios, and the resulting trajectories then compared with the control-scenario trajectories following the method described in Section 3.2. In the behaviour scenarios, characterized by several parameters, the parameters not being evaluated were kept constant at their lowest proposed value (e.g. 1.026 g/cm^3 for density and 0.3 m for size). The specific parameters in each scenario are detailed in Supplementary Material A.

Table 1. Model parameters, sensitivity values and key references.

Process/Behaviour		Model parameter	Value	Scenario	Comments and key references
Dispersion	Horizontal dispersion	Horizontal dispersion coefficient K_h, m^2/s	1 2 5 10	Control 1 2 3	Parameter value depends on the specific environment. We used the values proposed in *Critchell and Lambrechs (2016)*
	Vertical dispersion	Vertical dispersion coefficient K_v, m^2/s	10^{-5} 5×10^{-5} 10^{-4}	Control 4 5	Common values in marine systems *Talley et al., 2011*
Washing-off		Particle half-life on land before washing off *Tw* days	No washing off 1 2 No Monte Carlo	Control 6 7 8	Limited data. We used values of the same order of magnitude as in previous applications (*Liubartseva et al., 2018*), and included continuous washing-off at high tides (no Monte Carlo)
Sinking/ Behaviour	Physical properties	Density ρ g/cm^3	Passive 1.026 1.035 1.05 1.2 1.665	Control 9, 15 1, 16 11, 17 12, 18 13, 19	We selected density values commonly found in marine systems (*Khatmullina and Isachenko, 2017*): passive (e.g. polyethylene); 1.026 (near seawater density, e.g. some polystyrenes); 1.035 (e.g. acrylonitrile-butadiene-styrene); 1.05 (e.g. styrene-acrylonitrile); 1.2 (e.g. polycarbonate); 1.665 (e.g. polyester)
		Shape	Passive Sphere Cylinder	Control 9-13, 19-21, 25-27, 31-32, 36-37 14-18, 22-24, 28-30, 33-34, 39-40	Shapes with available formulations of settling velocity, *Katmullina and Isachinko (2017)*
		Size D or L mm*	Passive 0.3 1 2 5	Control 9, 14 19, 22 20, 23 21, 24	Microplastics are usually defined as particles ranging in size from 0.3 mm to 5 mm, *Hidalgo-Ruz et al. (2012)*
	Biofouling	Biofouling thickness *BT* g/cm^3	Passive 0 0.01 0.05 0.1	Control 9, 14 25, 28 26, 29 27, 30	*Chubarenko et al. (2016)* suggest values around 0.5 mm.
		Biofouling density *BD* g/cm^3	Passive 0 1.05 1.1 1.35	Control 9, 14 25, 28 31, 33 32, 34	Limited data. We used observed density values of observed biofouling layers in marine structures (*Macleod et al., 2016*). *Fisher et al. (1983)* suggest a value of 1.38 g/cm^3.
		Biofouling rate mm/day	Passive 0 0.0001 0.0005 0.01	Control 9, 14 35, 38 36, 39 37, 40	Limited data. Several studies suggest that biofouling can be visible after several days/weeks (*Ye and Andrady, 1991; Morét-Ferguson et al., 2010; Lobelle and Cunliffe, 2011*). We tried to reproduce this behaviour.
	Degradation	Degradation rate *DR*%	Passive 0 0.1 10 30	Control 19 41 42 43	Limited data. We used higher values than expected in coastal environments, just to gain insight into the importance of this process.

* The size of spheres and cylinders are defined by the diameter (*D*) and length (*L*), respectively. The cylinder diameter was constant in all the simulations at 0.3 mm.

The simulations were seeded at four locations (Fig. 2b): two inside the bay, in the inner region (R1) and around the entrance (R2); and two outside the bay, south (R3) and north (R4) of the entrance. These locations were strategically selected to reflect the constant transport of water into (warm surface inflow R3/R1) and out of (cold deep outflow R2/R4) the bay due to the cyclonic flow (see Fig. 2). Ten particles were released at each seeding site on 26 June 1998 for each scenario to compare the trajectories resulting from the different processes and behaviours. Simulations were run for 12 days, the mean residence time in the bay under low-exchange conditions (*Sun et al., 2017*), and provided the particle positions each hour.

3.2 Sensitivity analysis

The relative importance of each process and behaviour parameter was evaluated by comparing the trajectories of each scenario with those of the control scenario (passive particles, no washing-off and low dispersion). In order to avoid the random behaviour of turbulent dispersion having an impact on the comparison of scenarios, the same turbulent displacement was assigned to each particle at each time step for all scenarios, except for scenarios 1–3 (for K_h) and 4–5 (for K_v) that aimed to show the importance of turbulent dispersion on MPD trajectories (Table 1). We used three approaches to describe and quantify the differences between each scenario and the control: (1) visual and descriptive comparison of the resulting trajectories; (2) comparison of the percentage of particles reaching each of the three different types of fate — remaining suspended in the water, beached on land and settled to the bottom; (3) calculation of a dimensionless dynamical skill score that quantified the trajectory differences between each pair of scenarios over the whole duration of the experiments. We used a skill score (*ss*) based on the normalized cumulative Lagrangian separation (*Liu and Weisberg, 2001*) to compare the numerical and observed particle trajectories. This method has been frequently used to assess the performance of numerical ocean circulation models and oil-spill tracking models (*Röhrs et al., 2012; Liu et al., 2014; Sayol et al., 2014*). In this study, the skill score quantified the agreement between the trajectories of a given scenario and the trajectories of the control scenario, so that an *ss* close to 0 indicated a bad agreement, while an *ss* equal to 1 indicated that the trajectories were exactly the same. This allowed us to rank scenarios, and therefore to identify the processes and behaviours parameters that most affected the MPD trajectories and fates. Following *Liu and Weisberg (2001),* the skill score is defined as:

$$ss = \begin{cases} 1 - c/n & (c \leq n) \\ 0 & (c > n) \end{cases} \qquad (18)$$

where n is a tolerance threshold that defines the requirements of the comparison, so that a smaller value corresponds to stricter requirements and c is the normalized cumulative Lagrangian separation distance, calculated as the cumulative Lagrangian separation distance (d) divided by the cumulative length of the observed trajectory (l):

$$c = \sum_{i=1}^{N} d_i \Big/ \sum_{i=1}^{N} l_i, \qquad (19)$$

where i indicates the time step at which d and l were calculated, in this case every 12 hours during the trajectory period. We selected a tolerance threshold $n = 1$, following previous applications of this index (*Liu and Weisberg, 2001; Liu et al., 2014*). For each scenario, we calculated the *ss* of all the released particles, then the mean value for particles released at the same point.

3.3 Results and discussion

3.3.1 Relative impact of the physical processes

The MPD trajectories in all the scenarios differed from the control and from one another. All the modelled physical processes and behaviours therefore affected the transport of MPD, but to different degrees. The impact of each parameter on the trajectories also varied between the seeding locations (Fig. 2). Table 2 shows the skill scores and the percentages of the different type of particle fate (water, beach and bottom) for each scenario. These percentages are also shown in Fig. 3 for some key scenarios. As detailed in Section 3.2, *ss* quantifies the differences between the trajectories of the evaluated scenario and the control scenario. As each scenario represents the influence of one process or behaviour parameter, a low *ss* indicated a high impact of the evaluated parameter on the MPD trajectories and fates. In general, sinking and the behaviour parameters as a whole exhibited the lowest *ss* and therefore the biggest influence on the MPD transport, followed by turbulent dispersion and washing-off (Table 2).

Table 2. Skill Score and percentage of suspended, beached and settled particles for each sensitivity scenario. R1–R4 represent the four seeding sites (Fig. 2.c).

Physical processes and behaviour parameters		Scenario	Parameter value	Skill Score				Final Fate		
				R1	R2	R3	R4	Suspended (%)	Beached (%)	Settled (%)
Control								30	70	0
Horizontal turbulent dispersion	K_h	1	5 m^2/s	0.92	0.37	0.75	0.64	17.5	82.5	0
		2	10 m^2/s	0.82	0.35	0.70	0.57	12.5	87.5	0
		3	20 m^2/s	0.68	0.37	0.72	0.58	15	85	0
Vertical turbulent dispersion	K_v	4	5×10^{-5} m^2/s	0.88	0.52	0.81	0.67	20	77.5	2.5
		5	10^{-4} m^2/s	0.86	0.25	0.86	0.59	35	55	10
Washing-off	T_w	6	1 day	0.93	0.85	0.99	0.99	57.5	42.5	0
		7	2 day	0.93	0.85	0.99	0.99	75	25	0
		8	No Monte Carlo	0.91	0.81	0.99	0.99	77.5	22.5	0
Sinking/ Behaviour	ρ Sphere	9	1.026 g/cm^3	0.61	0.40	0.68	0.53	32.5	20	47.5
		10	1.035 g/cm^3	0.50	0.01	0.63	0.63	0	2.5	97.5
		11	1.05 g/cm^3	0.40	0.02	0.55	0.64	0	0	100
		12	1.2 g/cm^3	0.36	0.34	0.58	0.64	0	0	100
		13	1.665 g/cm^3	0.36	0.29	0.57	0.64	0	0	100
	ρ Cylinder	14	1.026 g/cm^3	0.57	0.24	0.67	0.53	50	25	25
		15	1.035 g/cm^3	0.43	0.02	0.58	0.58	0	0	100
		16	1.05 g/cm^3	0.39	0.02	0.56	0.64	0	0	100
		17	1.2 g/cm^3	0.36	0.29	0.57	0.64	0	0	100
		18	1.665 g/cm^3	0.36	0.29	0.57	0.64	0	0	100
	D Sphere	9	0.3 mm	0.61	0.40	0.68	0.53	32.5	20	47.5
		19	1 mm	0.48	0.00	0.66	0.63	0	0	100
		20	2 mm	0.39	0.01	0.58	0.64	0	0	100
		21	5 mm	0.36	0.34	0.58	0.64	0	0	100
	L Cylinder	14	0.3 mm	0.57	0.24	0.67	0.53	50	25	25
		22	1 mm	0.53	0.23	0.67	0.46	32.5	10	57.5
		23	2 mm	0.52	0.21	0.63	0.58	27.5	17.5	55
		24	5 mm	0.52	0.27	0.64	0.52	10	12.5	77.5
	BT Sphere	9	0 mm	0.61	0.40	0.68	0.53	32.5	20	47.5
		25	0.01 mm	0.57	0.10	0.59	0.62	0	17.5	82.5
		26	0.05 mm	0.39	0.02	0.54	0.64	0	0	100
		27	0.1 mm	0.38	0.07	0.56	0.64	0	0	100
	BT	14	0 mm	0.57	0.24	0.67	0.53	50	25	25

Cylinder	28	0.01 mm	0.57	0.10	0.62	0.57	0	17.5	82.5
	29	0.05 mm	0.40	0.03	0.57	0.65	0	0	100
	30	0.1 mm	0.39	0.01	0.58	0.64	0	0	100
	9	0 g/cm^3	0.61	0.40	0.68	0.53	32.5	20	47.5
BD Sphere	25	1.05 g/cm^3	0.57	0.10	0.59	0.62	0	17.5	82.5
	31	1.1 g/cm^3	0.41	0.03	0.70	0.63	0	0	100
	32	1.35 g/cm^3	0.38	0.20	0.57	0.64	0	0	100
	14	0 g/cm^3	0.57	0.24	0.67	0.53	50	25	25
BD Cylinder	28	1.05 g/cm^3	0.57	0.10	0.62	0.57	0	17.5	82.5
	33	1.1 g/cm^3	0.42	0.01	0.70	0.58	0	0	100
	34	1.35 g/cm^3	0.38	0.15	0.57	0.64	0	0	100
	9	0 mm/day	0.61	0.40	0.68	0.53	32.5	20	47.5
BR Sphere	35	0.001 mm/day	0.61	0.38	0.67	0.44	2.5	20	77.5
	36	0.005 mm/day	0.59	0.30	0.58	0.68	0	17.5	82.5
	37	0.01 mm/day	0.56	0.36	0.71	0.65	0	12.5	87.5
	14	0 mm/day	0.57	0.24	0.67	0.53	50	25	25
BR Cylinder	38	10^{-3} mm/day	0.58	0.23	0.59	0.57	2.5	15	82.5
	39	5 10^{-3} mm/day	0.57	0.24	0.54	0.62	0	7.5	92.5
	40	0.01 mm/day	0.54	0.33	0.69	0.63	0	12.5	87.5

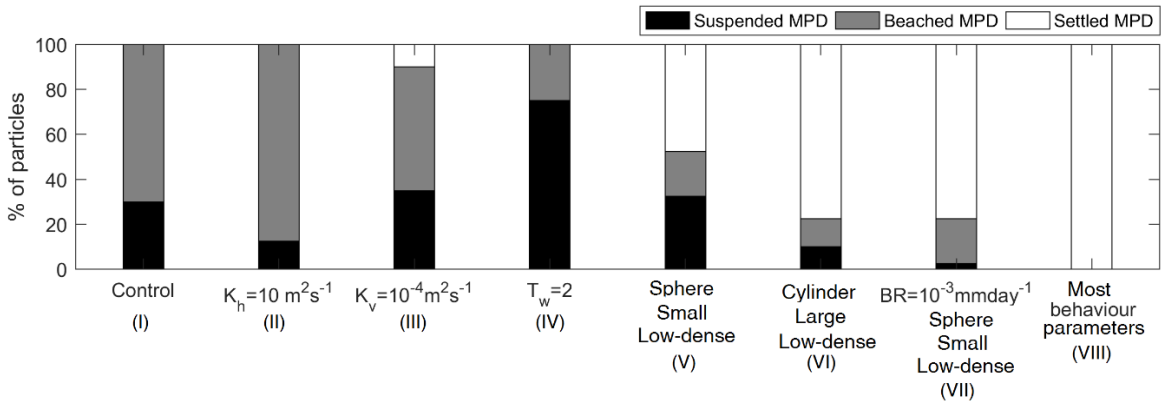

Fig. 3. Percentage of suspended, beached and settled MPD at the end of the simulation period (12 days) for scenarios representative of the different processes and behaviour parameters: control; horizontal dispersion (K_h = 10 m^2/s, Scenario 2); vertical dispersion (K_v = 10^{-4} m^2/s, Scenario 5); washing-off (T_w, Scenario 7); low-density small spheres (Scenario 10); low-density large cylinders (Scenario 25); low-density small spheres affected by non-stationary biofouling (BR = 10^{-3} mm/day Scenario 39); and most of the other behaviours (Scenarios 11–14, 16–22, 27–28, 30–35).

Washing-off

The washing-off scenarios had high values of *ss* (0.81–0.99), which reveals their similarity with the control (no washing-off, Table 2). In these scenarios, each particle followed the same trajectory as in the control, from the release time to their beaching (Fig. 4). After beaching, some particles were resuspended, others trapped on the coast. This was reflected by the higher percentage of suspended particles at the end of the simulation: 57.5–77% compared to 30% for the control (I and IV in Fig. 3, Table 2). Particles released in the bay (R1 and R2) beached sooner, so they had more opportunity to be washed off into the sea again, as reflected by the lower *ss* (0.81–0.93, Table 2). Despite this, these particles were beached on the east coast of the bay, which is characterized by low currents and residence times, so most of the washed-off particles remained in this region.

Particles released outside the bay stayed permanently in suspension or beached by the end of the simulation period. Their trajectories and final fates were therefore very similar to the control (*ss* near 1) but they could differ more and more with increased simulation times. The longer the MPD were

allowed to stay on land before being washed off (higher T_w or nullification of the Monte Carlo Method), the higher the probability of them then being washed-off. This was shown by the increase in settled particles with increasing T_w at the end of the simulation. However, the impact of higher washing-off probabilities on particle trajectories was barely captured by the *ss*. This was also due to the trapping of particles in the eastern region of the bay in all scenarios and the short simulation time, which prevented the washed-off particles moving away from the beaching locations.

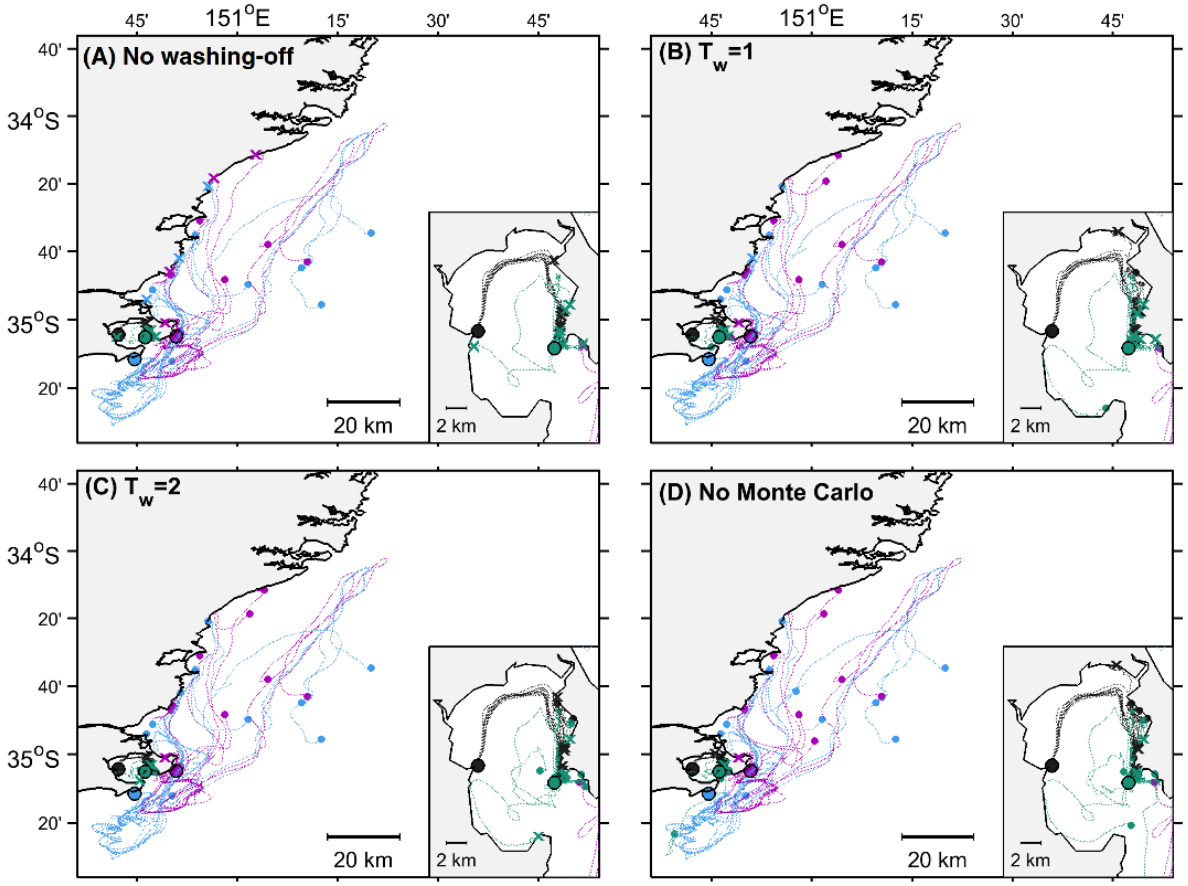

Fig. 4. Sources (circles), trajectories (lines) and fates, water (points), beach (crosses) and bottom (triangles), of MPD for the different washing-off scenarios (Tables 1 and 2): (**A**) no washing-off (control scenario); (**B**) T_w = 1 (Scenario 6); (**C**) T_w = 2 (Scenario 7); (**D**) no Monte Carlo Method (Scenario 8). The different colours represent MPD released at different sites: in the inner bay (R1, black); near the entrance (R2, green); south of the bay entrance (R3, blue); and north of the bay entrance (R4, pink).

Turbulent dispersion

Turbulence can be an important process in determining the trajectory and fate of the MPD. In general, an increase in the horizontal and vertical dispersion coefficients (K_h, K_v) increases the differences from the control trajectories (decreasing *ss*, Table 2), but the impact of these parameters depends to a large extent on the release point. Particles released in the inner bay (R1) followed the clockwise circulation of the bay for most values of K_h and K_v used, so the final fates of the MPD were very similar in all the scenarios (*ss* = 0.82–0.92, black lines and symbols in Fig. 5). Only a K_h of 20 m^2/s facilitated some

particles escaping from the main circulation and beach on the north coast of the bay (*ss* = 0.68, Fig. 5d). Particles released near the entrance (R2) stayed in the bay for all values of the dispersion coefficients and beached on the east coast of the bay (green lines and symbols in Fig. 5). However, higher K_v increased the probability of particles being displaced to the west by stratified currents, and then to the north coast of the bay by the clockwise circulation (Fig. 5e-f). In addition, larger K_v caused some of these particles to reach the bottom near the coast (III in Figs. 3, 5e-f). Despite these trajectories, any differences can be considered at first sight as relatively small; for different values of K_h in particular, the resulting *ss* was very low (0.25–37, Table 2). This can be explained by the fact that a third of the particles beached just after release at R2 in the control scenario. With increasing dispersion coefficients, these particles followed trajectories that, although short, resulted in a small *ss*.

The impact of the dispersion coefficients on the trajectories of particles released outside the bay was moderate (*ss* = 0.59–0.86, Table 2). Most of the particles released at these sites landed or were suspended in the same region north of Jervis Bay at the end of all the dispersion scenarios (blue and pink lines and symbols in Fig. 5). Increasing K_h enhanced the probability of particles released at R4 beaching on the north coast (II in Figs. 3, 5a-d); increasing K_v enhanced the probability of these same particles entering Jervis Bay (Fig. 5e-f).

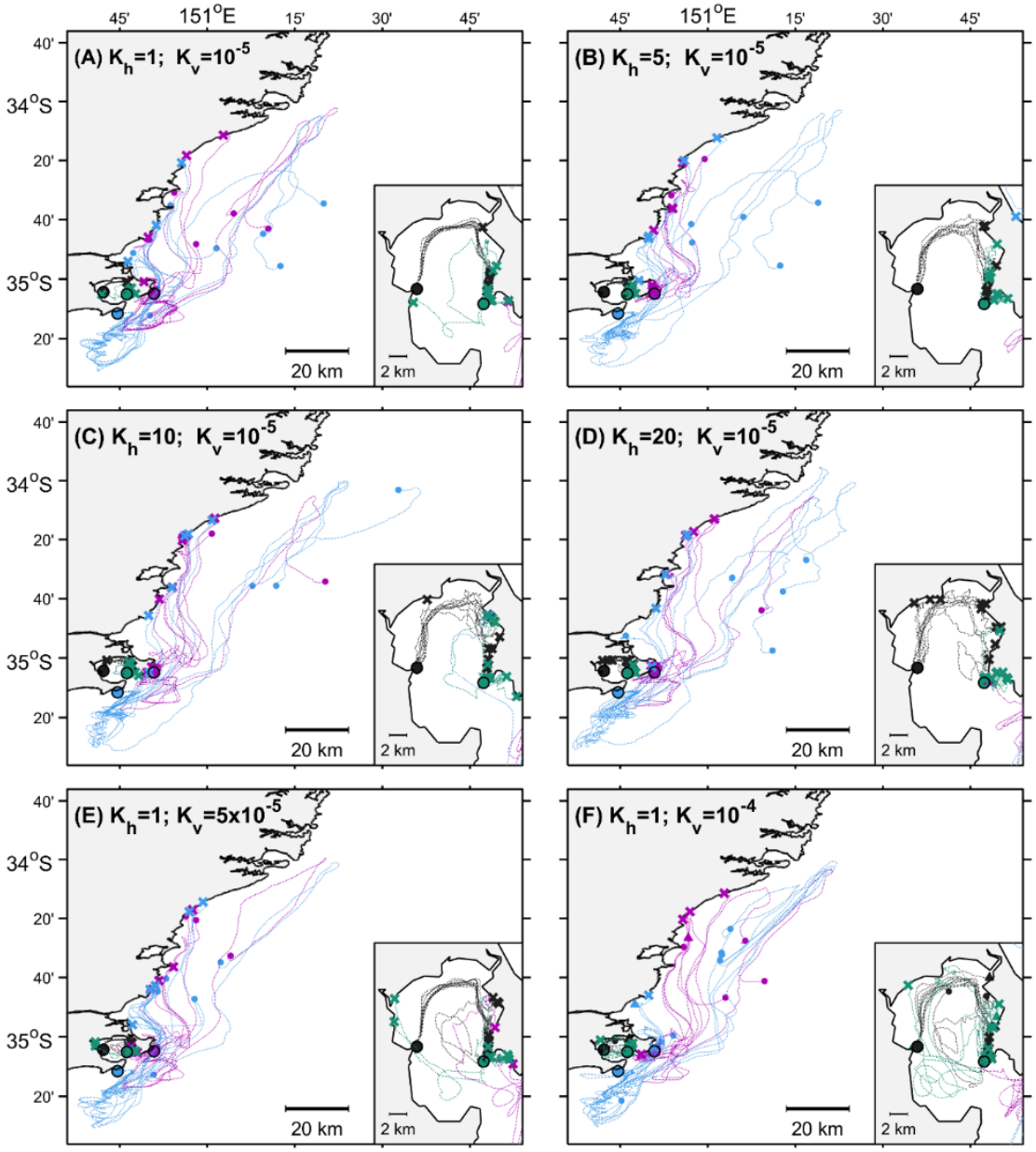

Fig. 5. Sources (circles), trajectories (lines) and fates, water (points), beach (crosses) and bottom (triangles), of MPD for the different dispersion scenarios (Table 1 and Supplementary Material): (**A**) K_h = 1 m^2/s and K_v = 10^{-5} m^2/s (control scenario); (**B**) K_h = 5 m^2/s and constant K_v (10^{-5} m^2/s) (Scenario 1); (**C**) K_h = 10 m^2/s and constant K_v (10^{-5} m^2/s) (Scenario 2); (**D**) K_h = 20 m^2/s and constant K_v (10^{-5} m^2/s) (Scenario 3); (**E**) constant K_h (1 m^2/s) and K_v= 5×10^{-5} m^2/s (Scenario 4); (**F**) constant K_h (1 m^2/s) and K_v = 10^{-4} m^2/s (Scenario 5). The different colours represent MPD released at different sites: in the inner bay (R1, black); near the entrance (R2, green); south of the bay entrance (R3, blue); and north of the bay entrance (R4, pink).

Sinking

MPD buoyancy had a dramatic impact on the model results (*ss* = 0.02–0.68). In most of the sinking scenarios, all the particles settled before the end of the simulation, except low-density cylinders, low-density small spheres and particles subject to progressive biofouling (Table 2, Fig. 3). This contrasted sharply with the control scenario results (70% and 30% of beached and suspended particles, respectively). The horizontal distribution of particles was therefore highly influenced by sinking,

particularly for particles released at the bay entrance (R2, Table 2, Figs. 6–10). These particles moved northward due to surface currents when they had a passive behaviour and beached along the eastern coast of the bay (Fig. 6a), whereas non-buoyant particles could be moved outside the bay by intermediate and bottom currents (Figs. 6b-d, 7b-d, see hydrodynamic description in Section 3.1). Particles released in the inner bay stayed inside the bay in all the scenarios, although their final fate depended on their behaviour (Figs. 6–10). Non-buoyant particles released outside the bay were also highly impacted by vertical gradients in the horizontal currents, so their trajectories and fates depended on the MPD behaviour. These results are in contrast with the modelling results of *Critchell and Lambrechts (2016),* who suggested that sinking has a relatively small influence on MPD fate. This is because they assumed that particles settle at a given rate (day^{-1}), and ignored the impact of the vertical current shear on the MPD transport as it moves vertically. The relative importance of each behaviour parameter affecting MPD transport is discussed further in Section 3.3.2.

3.3.2 Relative impact of behaviours

The trajectories in all behaviour scenarios differed to a large extent from the control, as highlighted by low *ss* values (Table 2, Fig. 11). Figure 11 compares the *ss* of the different behaviour scenarios (Table 2), showing the relative influence of the behaviour parameters (density, size, shape, and biofouling thickness, density and rate) on the MPD trajectories (for clarity, only values corresponding to particles released inside the bay, R1/R2, were included). This comparison suggests that, given the same release point, the relative importance of the different behaviour parameters was quite similar (similar order of magnitude of *ss*). All the behaviour parameters had a large impact on MPD transport, as all of them contributed to MPD buoyancy; however, the effect of some quantitative parameters, such as size, can vary according to the particle shape.

Physical properties: density, size and shape

The effect of increasing density (Fig. 6) and increasing size (Fig. 7) on the trajectories and fates of spherical MPD particles was very similar. Particles released in the inner bay (R1) were transported by the clockwise circulation in all the density and size scenarios (black lines in Figs. 6, 7). However, higher densities and sizes favoured an earlier sinking, and therefore a final fate closer to the release point but further away from the fate region of the control scenario. This was highlighted by the decrease in *ss* as density or size increased (R1 spheres in Fig. 11a-b).

Spherical particles released near the entrance (R2) exhibited different trajectories, depending on their density and size: **(a)** passive particles beached after a few hours close to the release point (green crosses, Figs. 6a, 7a); **(b)** some small particles with a density slightly higher than that of water also

beached near the release point, but others were transported to the west by the inflow current near the surface (green lines, Figs. 6b, 7b); (**c**) particles with intermediate densities (1.035–1.05 g/cm^3, green lines in Fig. 6c-d) and sizes (1–2 mm, green lines in Fig. 7c-d) were transported out of the bay by deep outflow currents (an *ss* near 0 indicates a large difference from the control trajectories, R2 spheres in Fig. 11a-b); (**d**) high-density (>1.2 g/cm^3, Fig. 6e-f) and big particles (5mm, Fig. 7e) settled quickly and near the release point (higher *ss* than intermediate densities and sizes, R2 spheres in Fig. 11a-b).

Particles released outside the bay (R3/R4) were also significantly influenced by density and size. Low-density small particles (pink and blue, Figs. 6b, 7b) were transported to the north region, as passive particles (pink and blue, Figs. 6a, 7a), but settled before reaching the coast or were about to settle by the end of the simulation. Some of this type of particle were also transported inside the bay by surface inflow currents. Particles with intermediate densities and sizes (pink and blue, Figs. 6c-d, 7c-d) were transported to the northeast by intermediate and deep strong currents, travelling long distances in some cases (e.g. blue lines in Fig. 6c). This agrees with some experimental studies that suggest that non-buoyant MPD might travel longer distances than buoyant MPD due to hydrodynamic mixing processes (*Frére et al., 2017; Zhang, 2017*). Very high densities and sizes led particles to sink quickly near the release point (pink and blue, Figs. 6e-f, 7e).

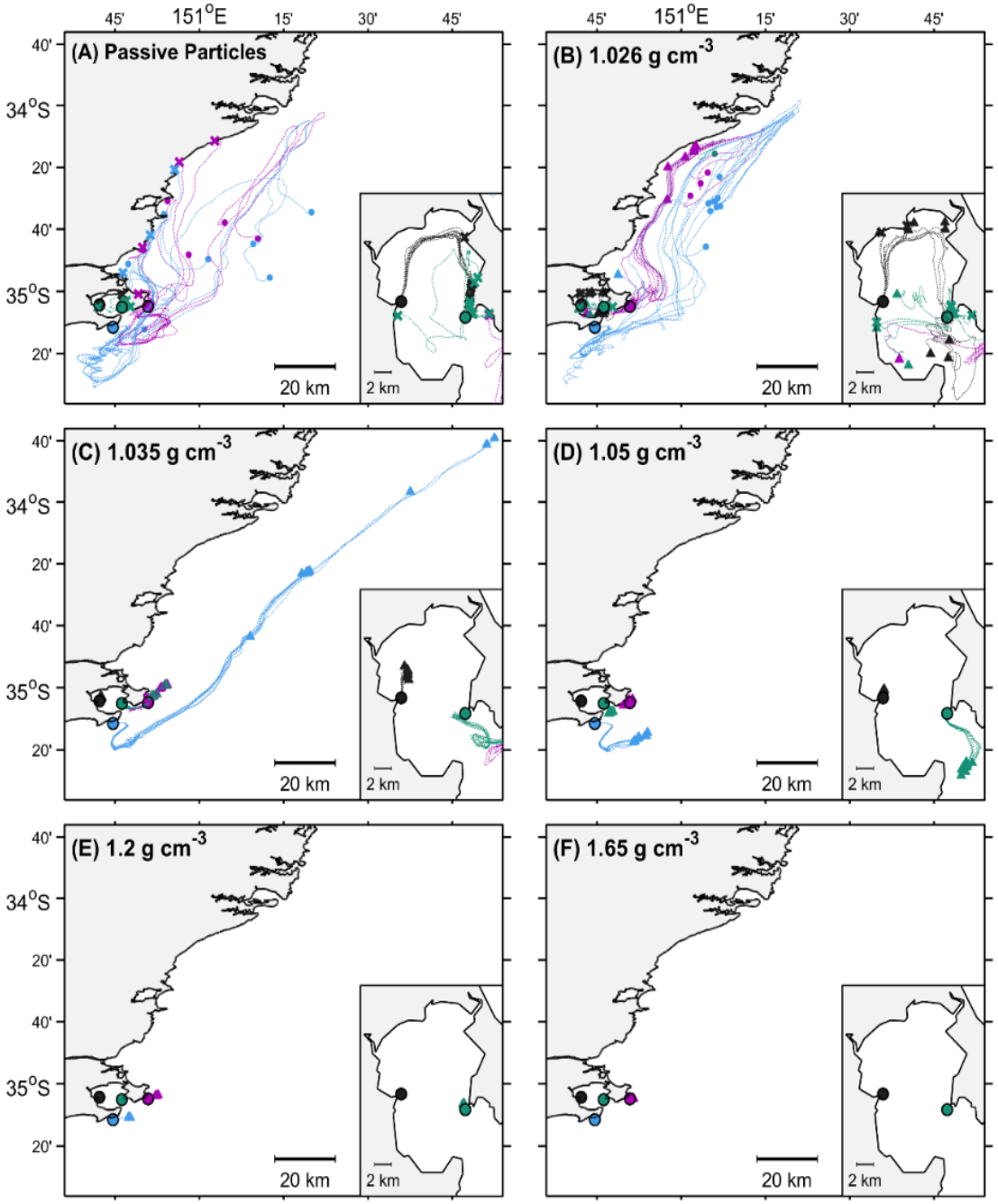

Fig. 6. Sources (circles), trajectories (lines) and fates, water (points), beach (crosses) and bottom (triangles), of MPD for the scenarios with spheres of different densities (Table 1 and Supplementary Material): (**A**) passive particles (control scenario); (**B**) ρ = 1.026 g/cm^3 (Scenario 10); (**C**) ρ = 1.035 g/cm^3 (Scenario 11); (**D**) ρ = 1.05 g/cm^3 (Scenario 12); (**E**) ρ = 1.2 g/cm^3 (Scenario 13); (**F**) ρ = 1.665 g/cm^3 (Scenario 14). All particles had diameter 0.33 mm. The different colours represent MPD released at different sites: in the inner bay (R1, black); near the entrance (R2, green); south of the bay entrance (R3, blue); and north of the bay entrance (R4, pink).

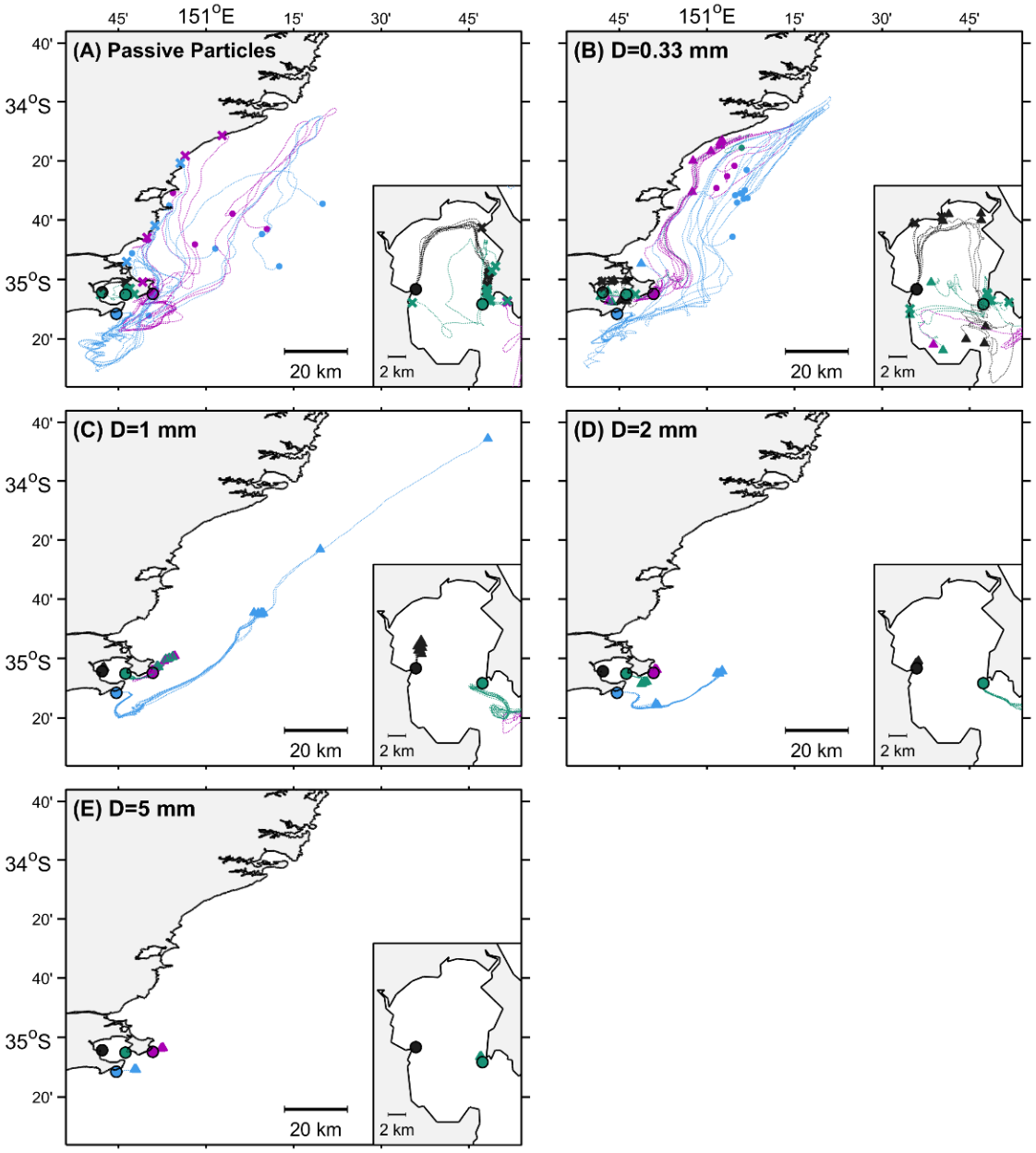

Fig. 7. Sources (circles), trajectories (lines) and fates, water (points), beach (crosses) and bottom (triangles), of MPD for the scenarios with spheres of different size (Table 1 and Supplementary Material): (**A**) passive particles (control scenario); (**B**) D = 0.33 mm (Scenario 9); (**C**) D = 1 mm (Scenario 19); (**D**) D = 2 mm (Scenario 20); (**E**) D = 5 mm (Scenario 21). All particles had a density of 1.026 g/cm^3. The different colours represent MPD released at different sites: in the inner bay (R1, black); near the entrance (R2, green); south of the bay entrance (R3, blue); and north of the bay entrance (R4, pink).

The impact of density on the trajectories of cylindrical MPD was the same as for spherical MPD. Cylindrical particles followed similar paths to spherical particles for each density value and each release site (see trajectories of Scenarios 15–19 in Supplementary Material B). This is shown in Fig. 11a; *ss* values were similar for the trajectories of the spherical and cylindrical particles. The behaviour of cylindrical particles of different sizes was, in contrast, completely different from that of spherical particles. For the same density, cylindrical particles released at the same site all followed similar trajectory patterns, regardless of size. These patterns were the following (ρ = 1.026 g/cm^3 and all

cylinder lengths; Fig. 8): particles released at R1 were transported by the clockwise circulation and settled on the north coast of the bay; particles released at R2 settled near the release site or were transported to the western coast of the bay by near-surface currents; and particles released at R3 and R4 were transported to the north, where they settled, or were about to settle, by the end of the simulation. Unlike spheres, not all the cylindrical medium- and large-size particles settled by the end of the simulations (compare VI and VIII in Fig. 3, Table 2). This lack of an effect of increasing size on the trajectories of cylindrical particles was also evidenced by the constant values of *ss* for all the scenarios with cylinders of different sizes (all showed a similar difference from the control trajectories, Fig. 11b), and by the moderate increase in the percentage of settled particles with size (Table 2, Scenario in Fig. 3). This was a direct consequence of the settling-velocity equation used for these particles (*Katmullina and Isachinko, 2017*, Section 2.2.3), which is based on the observation of different behaviours for cylindrical and spherical MPD. While the behaviour of spherical particles depends on both density and size, the behaviour of cylindrical MPD mainly depends on the density.

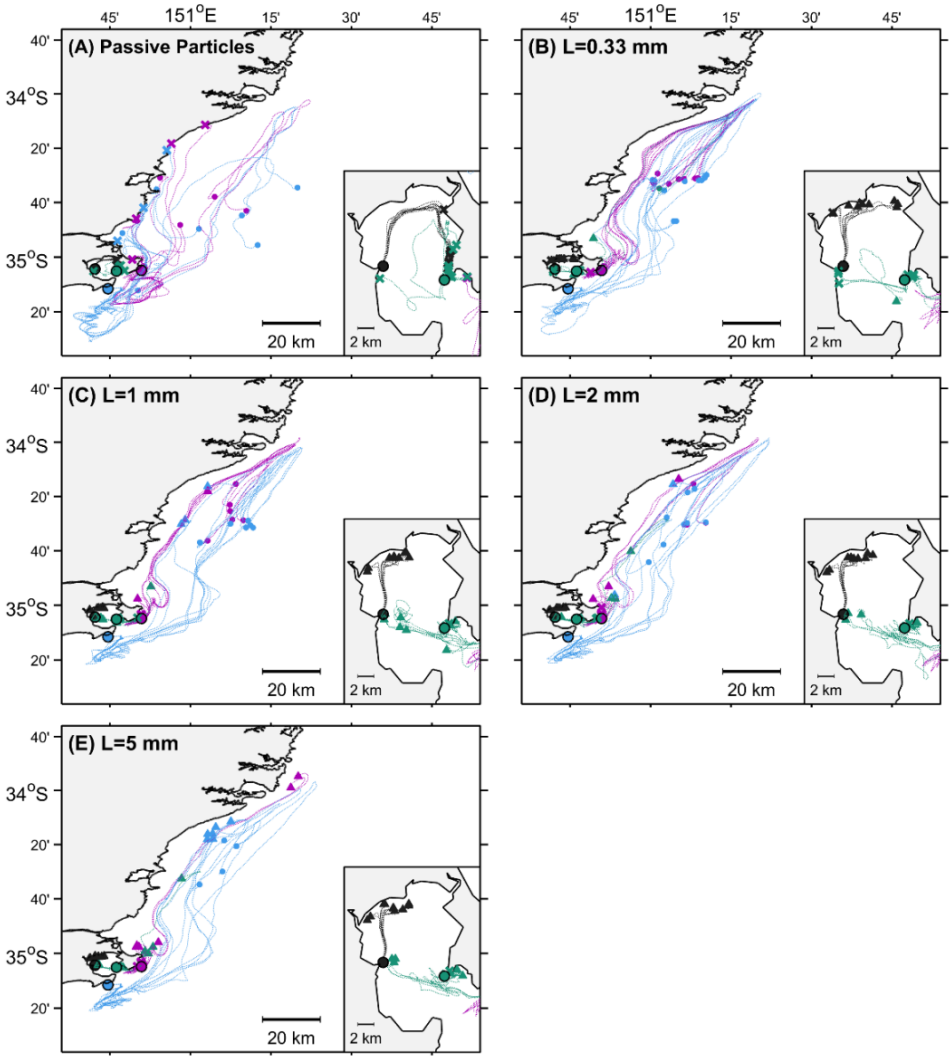

Fig. 8. Sources (circles), trajectories (lines) and fates, water (points), beach (crosses) and bottom (triangles), of MPD for the scenarios with cylinders of different sizes (Table 1 and Supplementary Material): (**A**) passive particles (control scenario); (**B**) *L*

= 0.33 mm (Scenario 14); (**C**) *L* = 1 mm (Scenario 22); (**D**) *L* = 2 mm (Scenario 23); (**E**) *D* = *L* (Scenario 24). All the particles had a constant density of 1.026 g/cm^3. The different colours represent MPD released at different sites: in the inner bay (R1, black); near the entrance (R2, green); south of the bay entrance (R3, blue); and north of the bay entrance (R4, pink).

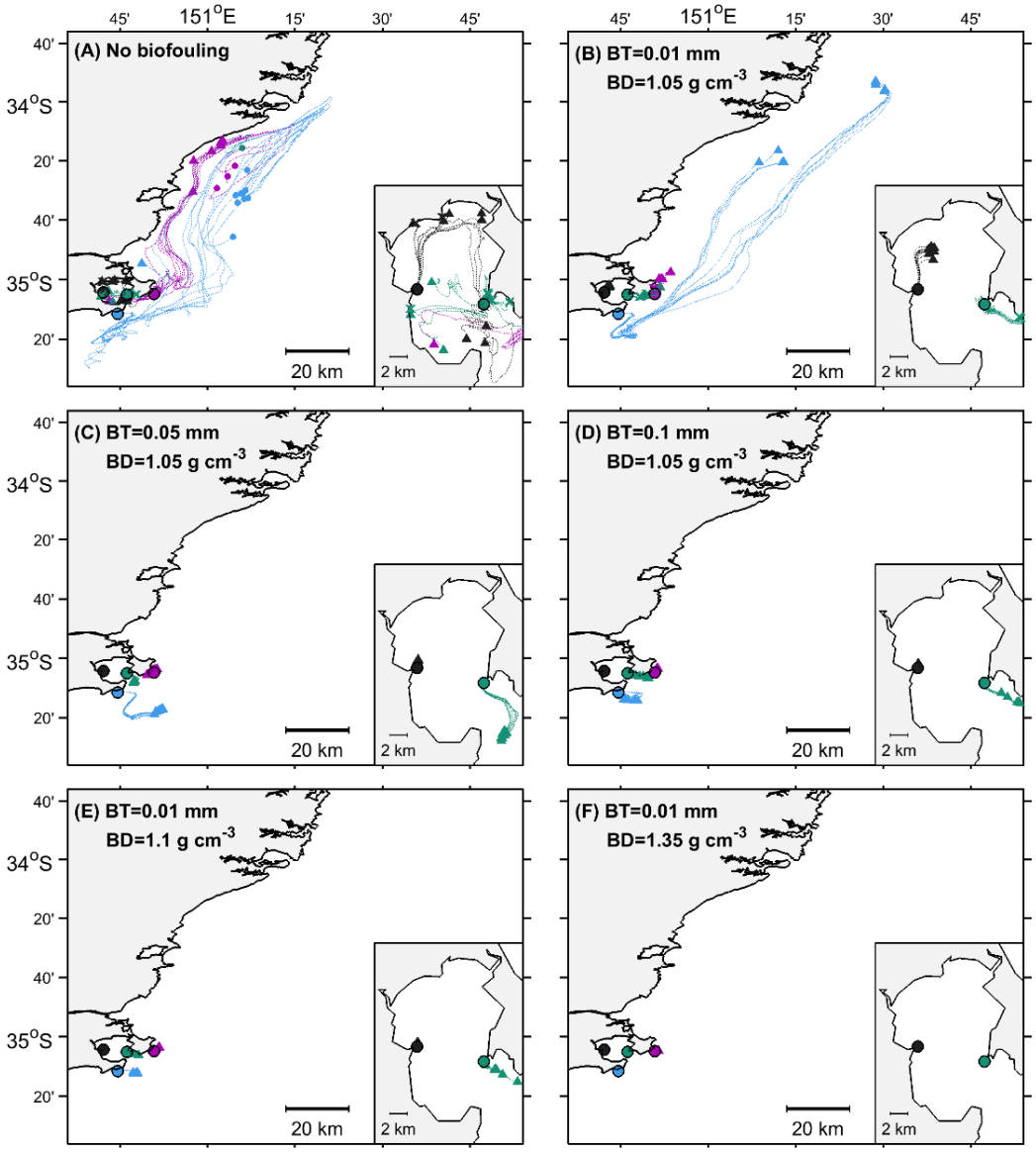

Fig. 9. Sources (circles), trajectories (lines) and fates, water (points), beach (crosses) and bottom (triangles), of MPD for the scenarios with spheres subject to stationary biofouling (Table 1 and Supplementary Material): (**A**) no biofouling (Scenario 9); (**B**) *BT* = 0.01 mm and *BD* = 1.05 g/cm^3 (Scenario 25); (**C**) *BT* = 0.05 mm and *BD* = 1.05 g/cm^3 (Scenario 26); (**D**) *BT* = 0.1 mm and *BD* = 1.05 g/cm^3 (Scenario 27); (**E**) *BT* = 0.01 mm and *BD* = 1.1 g/cm^3 (Scenario 31); (**F**) *BT* = 0.01 mm and *BD* = 1.35 g/cm^3 (Scenario 32). All the particles had an initial density of 1.026 g/cm^3 and an initial size of 0.33 mm. The different colours represent MPD released at different sites: in the inner bay (R1, black); near the entrance (R2, green); south of the bay entrance (R3, blue); and north of the bay entrance (R4, pink).

Biofouling

The effect of different fouling states on MPD transport was analysed by varying the biofilm thickness (*BT*), with a relatively low biofilm density (1.05 g/cm^3), and varying the biofilm densities (*BD*), with a relatively small biofilm thickness (0.01 mm), of particles with a constant density and size (Table 1 and Supplementary Material A). The trajectories in the biofouling scenarios differed to a larger extent from

the control than the trajectories in the scenario free of biofouling, for both spherical and cylindrical particles (lower *ss*, Fig. 11b-c, Table 2). This revealed the large influence of this bio-physical process on MPD motion and fate. Figure 9 compares the trajectories of these scenarios for spherical particles. In most cases, biofouling led to a significant increase in the settling velocity, and particles settled very soon in this shallow system (Fig. 9c-f). Only particles released at R3 and characterized by a low biofilm thickness and density (blue lines, Fig. 9b) travelled longer distances through deeper waters before settling, carried by a strong intermediate current. Cylindrical particles showed very similar behaviour and trajectories to spherical particles (similar *ss*, Fig. 11c-d, see trajectories in Supplementary Material B). This is because the trajectories and fates of both spherical and cylindrical particles were very sensitive to density, and biofilms are characterized by densities much higher than water (*Fisher et al. 1983*). The main difference was that cylindrical MPD released at R3 did, in general, travel slight longer distances due to the slightly lower settling velocity of cylindrical fouled particles compared to spherical.

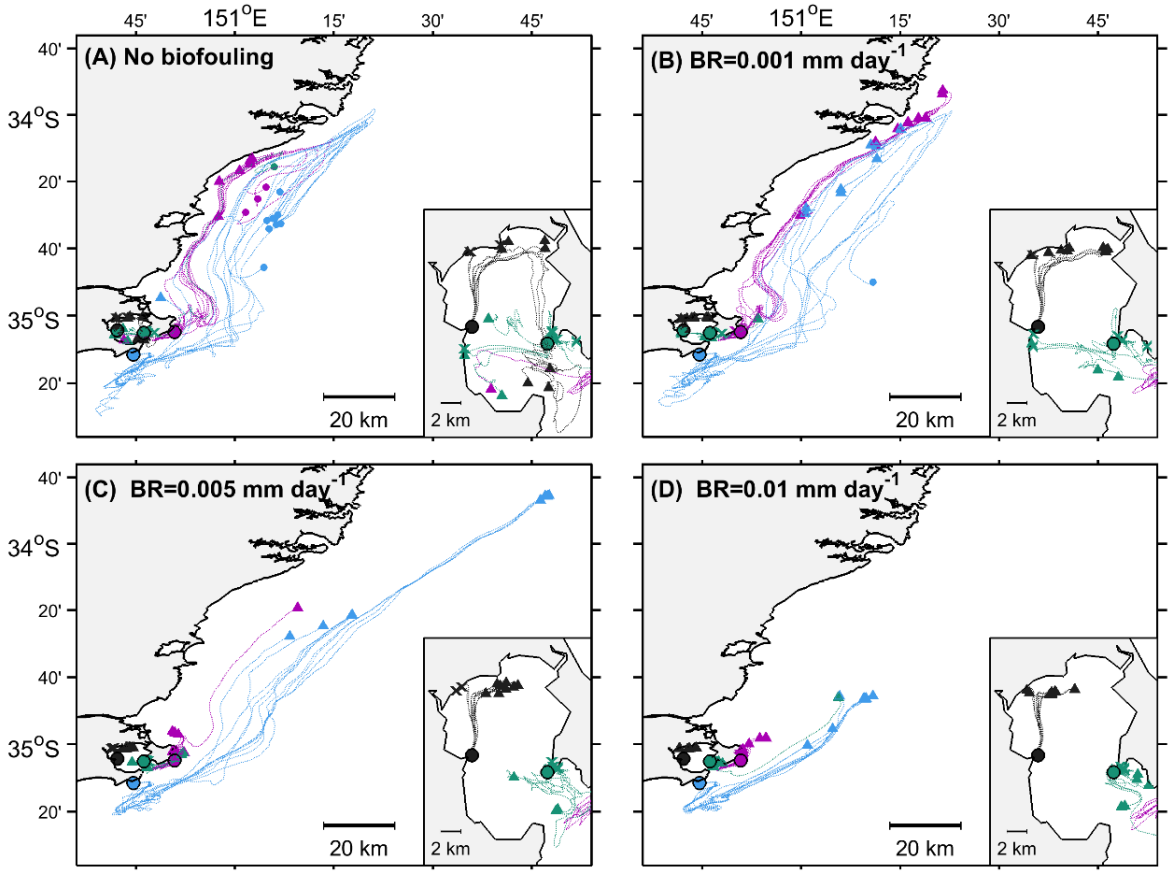

Fig. 10. Sources (circles), trajectories (lines) and fates, water (points), beach (crosses) and bottom (triangles), of MPD for the scenarios with spheres subject to non-stationary biofouling (Table 1 and Supplementary Material): (**A**) no biofouling (Scenario 9);(**B**) *BR* = 0.001 mm/day (Scenario 35); (**C**) *BR* = 0.005 mm/day (Scenario 36); (**D**) *BR* = 0.01 mm/day (Scenario 37). All the particles had an initial density of 1.026 g/cm^3 and an initial size of 0.33 mm. The different colours represent MPD released at different sites: in the inner bay (R1, black); near the entrance (R2, green); south of the bay entrance (R3, blue); and north of the bay entrance (R4, pink).

These results demonstrate that both biofouling parameters, biofilm thickness and density, played an important role in the behaviour of MPD. However, biofouling is a non-stationary process, so biofouling thickness can vary over time. As explained in Section 2.2.3, a progressive increase in the biofouling thickness was parameterized by a constant biofilm rate (*BR*, mm/day) in order to gain insight into the sensitivity of the MPD transport to this process. Trajectories and fates of particles subjected to very small *BR* (0.001 mm/day) were very similar to those of particles free of biofouling (Fig. 10a-b, similar *ss*, Fig. 11e), although with some differences. Some particles with a small BR, released near the entrance (R2), were displaced outside the bay before sinking, caused by the deeper outflow currents; particles released outside the bay (R3/R4) settled sooner and further north. This was highlighted by the increase in the percentage of settled particles by the end of the simulation (compare V and VII in Fig. 3). As *BR* increased, particles showed a behaviour closer to that of more-dense or large particles (Fig. 10c-d). For example, particles released at R2 were flushed out of the bay. These conclusions are valid for both spherical (Fig. 10) and cylindrical particles (see trajectories in Supplementary Material B). These results demonstrate that progressive changes in the biofilm thickness can impact MPD transport. Therefore, for accurate predictions of MPD fate, the MPD tracking models need to be fed with realistic estimates of biofilm variability (*Kooi et al., 2017*), which in turns requires prioritizing laboratory and field studies in this area.

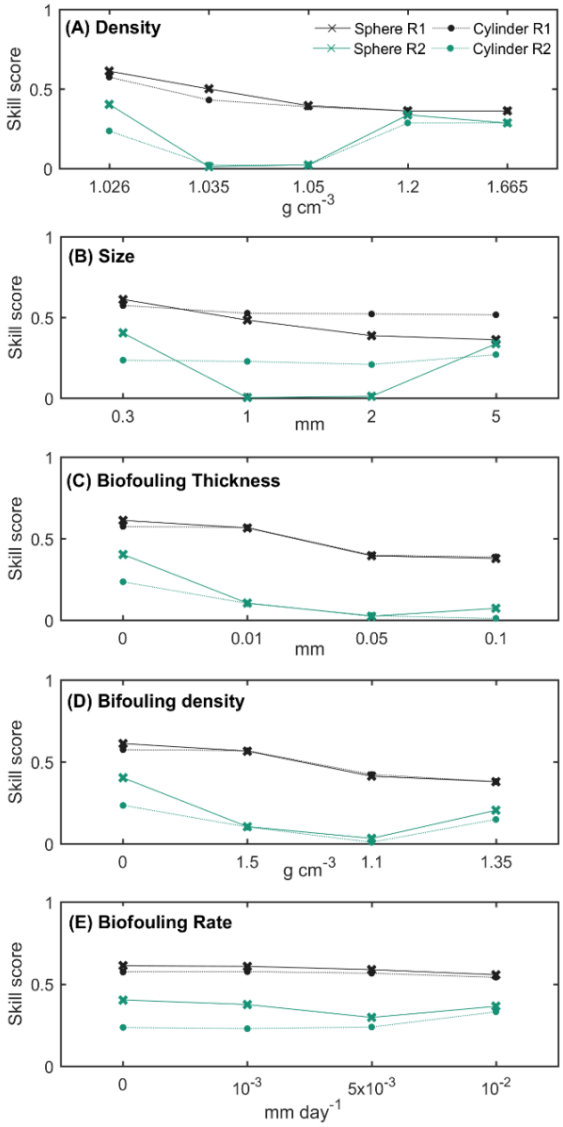

Fig. 11. Skill scores of scenarios modelling the effect of the behaviour parameters (see values in Table 2): (**A**) density (Scenarios 9–18); (**B**) size (Scenarios 9, 14, 19–24); (**C**) biofouling thickness (Scenarios 9, 14, 25–30); (**D**) biofouling density (Scenarios 9, 14, 25, 28, 31–34); (**E**) biofouling rate (Scenarios 9, 14, 35–40). The different colours represent MPD released at different sites: in the inner bay (R1, black) and near the entrance (R2, green). Crosses and dots represent spherical and cylindrical particles, respectively.

Degradation

As explained in Section 3.1, degradation was not included in the sensitivity analysis since it is a slower process that needs a more accurate parameterization. Nevertheless, we compared the trajectories of particles subject to different (overstated) degradation rates, representing a constant loss of size (*DR*% size decrease per day, Section 2.2.3), in order to provide some insight into its influence on MPD trajectories and fates (Fig. 12). All these scenarios were characterized by a density of 1.026 g/cm^3, an initial size of 1 mm and spherical shape (see details in Supplementary Material A). Particles subject to both small (0.1% per day, Fig. 12b) and high (10% per day, Fig. 12c) degradation rates showed the same behaviour as particles free of degradation (Fig. 12c). Only some particles, with a *DR* of 30% per

day, followed different paths, as the loss of size favoured a retarded sinking and therefore transport into deeper water by a strong intermediate current (blue and green lines in Fig. 12d). The slow loss of size had only a small influence on the transport of non-buoyant MPD in relatively shallow systems, but improved experimental and modelling parameterization are necessary to investigate this further. An instantaneous fragmentation of particles may have a higher impact on the transport of MPD, as particles with different sizes can have very different behaviours (Fig. 7). This process will be included in future versions of TrackMPD once there is a better understanding.

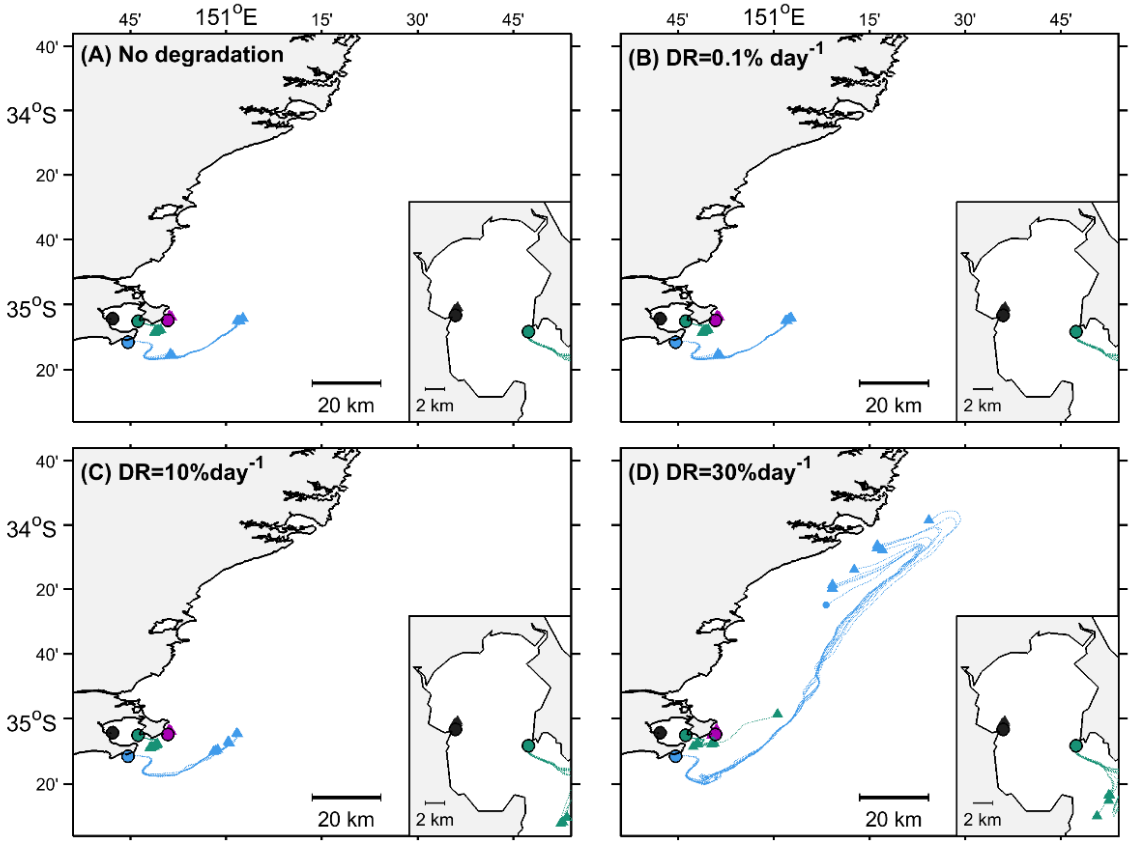

Fig. 12. Sources (circles), trajectories (lines) and fates, water (points), beach (crosses) and bottom (triangles), of MPD for the scenarios subject to degradation (Table 1 and Supplementary Material): (**A**) no degradation (Scenario 19); (**B**) *DR* = 0.1% per day (Scenario 41); (**C**) *DR* = 10% per day (Scenario 42); (**D**) *DR* = 20% per day (Scenario 43). All the particles had a density of 1.026 g/cm^3, an initial size of 1 mm and spherical shape. The different colours represent MPD released at different sites: in the inner bay (R1, black), near the entrance (R2, green); south of the bay entrance (R3, blue); and north of the bay entrance (R4, pink).

4. Conclusions

TrackMPD provides a comprehensive, user-friendly, and versatile environment for the modelling of marine plastic transport in coastal and marine systems. We have demonstrated that the proposed modelling framework fills the gaps in previous models by: (1) considering a three-dimensional approach; (2) providing compatibility with a variety of ocean models; and (3) including a wide range of

physical processes (advection, dispersion, windage, sinking, settling, beaching and washing-off) and MPD behaviour that depend on particle dynamical properties, and the fouling and degradation state. The modular structure allows users to select and adjust the processes and behaviours included in a simulation, and favours the future replacement of model formulations in line with experimental progress.

Through a sensitivity analysis of the model parameters, we have demonstrated the large influence of the proposed physical processes and behaviours on the transport and fate of MPD, and thus the relevance of a three-dimensional modelling approach. Sinking had a dramatic impact on MPD trajectory and fate, followed by turbulent dispersion and washing-off. The relative importance of all the model behaviour parameters influencing the MPD trajectories was quite similar. Density, size and shape determine MPD buoyancy, which played a key role in the vertical transfer of particles between the vertical shear layers and on the settling of particles, especially in shallow waters. The behaviour of spherical particles was determined by density and size, while the behaviour of cylindrical particles mainly depended on density. Biofouling thickness and density had a strong influence in decreasing MPD buoyancy and thereby impacting MPD motion. Preliminary results on the impact of time-varying biofouling and degradation suggest that a progressive increase in biofouling thickness may have a significant influence on MPD paths and fates, while the progressive decrease in size due to degradation seems to have only a slight influence, particularly in shallow systems.

In addition to accurate hydrodynamic data, the successful estimation and prediction of MPD sources, paths, distribution and accumulation zones using TrackMPD, and numerical models in general, require accurate in-situ measurements of model parameters. At the very least, drifter data to estimate the dispersion coefficients and validate trajectories, and microplastic samples to evaluate the particle physical properties are required. Combining surface and subsurface drifter experiments could help to assess particle behaviour in turbulent and stratified environments. Our modelling results also highlight the need for priority research on biofouling parameterization to better understand and predict MPD movement. Improvements in parameterizing and quantifying rates of other biological and physical processes and behaviours such washing-off, resuspension, degradation, fragmentation and animal ingestion are also critical to progress in this issue. Future ambitions for the model involve the compatibility with unstructured grids, and the improvement or new development of processes and behaviour formulations. A priority will be to better parameterize non-stationary biofouling and the washing-off, and include plastic fragmentation and bottom resuspension.

Acknowledgments

The authors thank Nick Goldie and Dr Peter McIntyre for proofreading the article. The authors also acknowledge the reviewers for their useful comments. This is publication no. 56 of SARCCM at UNSW Canberra. Professor Erick Fredj was supported by a SARCCM Visiting Fellow Grant. This

work was supported by Intersect, the National Computational Infrastructure National Facility at the Australian National University and by UNSW LIEF grant share LE120100181. The code source will be published under GPL licence and, in the meantime, can be requested from authors.

References

Al-Rabeh, A.H., Lardner, R.W., Gunay, N., 2000. Gulfspill Version 2.0: A software package for oil spills in the Arabian Gulf. Environ. Model. Softw. 15, 425–442. https://doi.org/10.1016/S1364-8152(00)00013-X

Anderson, E., Odulo, A., Spaulding, M., 1998. Modeling of Leeway Drift. U.S. Coast Guard Res. Dev. Cent. Rep. GC-D-06-09.

Andrady, A. L., 2011. Microplastics in the marine environment, Mar. Pollut. Bull. 62(8), 1596–1605, https://doi:10.1016/j.marpolbul.2011.05.030.

Bagaev, A., Mizyuk, A., Khatmullina, L., Isachenko, I. and Chubarenko, I., 2017. Anthropogenic fibres in the Baltic Sea water column: Field data, laboratory and numerical testing of their motion, Sci. Total Environ., 599–600:560–571. https://doi:10.1016/j.scitotenv.2017.04.185.

Ballent, A., Purser, A., de Jesus Mendes, P., Pando, S., Thomsen, L., 2012. Physical transport properties of marine microplastic pollution. Biogeosciences Discuss. 9, 18755–18798. https://doi.org/10.5194/bgd-9-18755-2012

Barnes, D.K.A., 2002. Invasions by marine life on plastic debris. Nature 416, 808–809. https://doi.org/10.1038/416808a

Barnes, D.K.A., Galgani, F., Thompson, R.C., Barlaz, M., 2009. Accumulation and fragmentation of plastic debris in global environments. Phil. Trans. R. Soc. B Biol. Sci. 364, 1985–1998. https://doi.org/10.1098/rstb.2008.0205

Browne, M.A., Galloway, T.S., Thompson, R.C., 2010. Spatial patterns of plastic debris along estuarine shorelines. Environ. Sci. Technol. 44, 3404–3409. https://doi.org/10.1021/es903784e

Browne, M.A., Niven, S.J., Galloway, T.S., Rowland, S.J., Thompson, R.C., 2013. Microplastic moves pollutants and additives to worms, reducing functions linked to health and biodiversity. Curr. Biol. 23, 2388–2392. https://doi.org/10.1016/j.cub.2013.10.012

Carlson, D.F., Suaria, G., Aliani, S., Fredj, E., Fortibuoni, T., Griffa, A., Russo, A., Melli, V., 2017. Combining litter observations with a regional ocean model to identify sources and sinks of floating debris in a semi-enclosed basin: The Adriatic Sea. Front. Mar. Sci. 4(78). https://doi.org/10.3389/fmars.2017.00078

Chubarenko, I., Bagaev, A., Zobkov, M., Esiukova, E., 2016. On some physical and dynamical properties of microplastic particles in marine environment. Mar. Pollut. Bull. 108, 105–112. https://doi.org/10.1016/j.marpolbul.2016.04.048

Clark, J.R., Cole, M., Lindeque, P.K., Fileman, E., Blackford, J., Lewis, C., Lenton, T.M., Galloway, T.S., 2016. Marine microplastic debris: a targeted plan for understanding and quantifying interactions with marine life. Front. Ecol. Environ. 14, 317–324. https://doi.org/10.1002/fee.1297

Cole, M., 2016. A novel method for preparing microplastic fibers. Sci. Rep. 6, 34519. https://doi.org/10.1038/srep34519

Critchell, K., Lambrechts, J., 2016. Modelling accumulation of marine plastics in the coastal zone; what are the dominant physical processes? Estuar. Coast. Shelf Sci. 171, 111–122. https://doi.org/10.1016/j.ecss.2016.01.036

Derraik, J.G.B., 2002. The pollution of the marine environment by plastic debris: A review. Mar. Pollut. Bull. 44(9), 842-852. https://doi.org/10.1016/S0025-326X(02)00220-5

Doyle, M.J., Watson, W., Bowlin, N.M., Sheavly, S.B., 2011. Plastic particles in coastal pelagic ecosystems of the Northeast Pacific ocean. Mar. Environ. Res. 71, 41–52. https://doi.org/10.1016/j.marenvres.2010.10.001

Ebbesmeyer, C.C., Ingraham, W.J., Jones, J.A., Donohue, M.J., 2012. Marine debris from the Oregon Dungeness crab fishery recovered in the northwestern Hawaiian Islands: Identification and oceanic drift paths. Mar. Pollut. Bull. 65, 69–75. https://doi.org/10.1016/j.marpolbul.2011.09.037

Efimova, I., Bagaeva, M., Bagaev, A., Kileso, A. and Chubarenko I., 2018. Secondary microplastics generation in the sea swash zone with coarse bottom sediments: Laboratory experiments. Front. Mar. Sci. 5(313). http://doi: 10.3389/fmars.2018.00313

Enders, K., Lenz, R., Stedmon, C.A., Nielsen, T.G., 2015. Abundance, size and polymer composition of marine microplastics ≥10μm in the Atlantic Ocean and their modelled vertical distribution. Mar. Pollut. Bull. 100, 70–81. https://doi.org/10.1016/j.marpolbul.2015.09.027

Eriksen, M., Lebreton, L.C.M., Carson, H.S., Thiel, M., Moore, C.J., Borerro, J.C., Galgani, F., Ryan, P.G., Reisser, J., 2014. Plastic pollution in the world's oceans: More than 5 trillion plastic pieces weighing over 250,000 tons afloat at sea. PLoS One 9(12). https://doi.org/10.1371/journal.pone.0111913

Filella, M., 2015. Questions of size and numbers in environmental research on microplastics: Methodological and conceptual aspects. Environ. Chem. 12, 527–538. https://doi.org/10.1071/EN15012

Fisher, N.S., Bjerregaard, P., Fowler, S.W., 1983. Interactions of marine plankton with transuranic elements. 1. Biokinetics of neptunium, plutonium, americium, and californium in phytoplankton. Limnol. Oceanogr. 28, 432–447. https://doi.org/10.4319/lo.1983.28.3.0432

Fredj, E., Carlson, D.F., Amitai, Y., Gozolchiani, A., Gildor, H., 2016. The particle tracking and analysis toolbox (PaTATO) for Matlab. Limnol. Oceanogr. Methods 14, 586–599. https://doi.org/10.1002/lom3.10114

Frére, L., Paul-Pont, I., Rinnert, E., Petton, S., Jaffré, J., Bihannic, I., Soudant, P., Lambert, C., Huvet, A., 2017. Influence of environmental and anthropogenic factors on the composition, concentration and spatial distribution of microplastics: A case study of the Bay of Brest (Brittany, France). Environ. Pollut. 225, 211–222. https://doi.org/10.1016/j.envpol.2017.03.023

Gajšt, T., Bizjak, T., Palatinus, A., Liubartseva, S., Kržan, A., 2016. Sea surface microplastics in Slovenian part of the Northern Adriatic. Mar. Pollut. Bull. 113, 392–399. https://doi.org/10.1016/j.marpolbul.2016.10.031

Gall, S.C., Thompson, R.C., 2015. The impact of debris on marine life. Mar. Pollut. Bull. 92, 170–179. https://doi.org/10.1016/j.marpolbul.2014.12.041

Gilfillan, L.R., Ohman, M.D., Doyle, M.J., Watson, W., 2009. Occurrence of plastic micro-debris in the southern California Current system. Calif. Coop. Ocean. Fish. Investig. Reports 50, 123–133.

Gregory, M.R., 2009. Environmental implications of plastic debris in marine settings-entanglement, ingestion, smothering, hangers-on, hitch-hiking and alien invasions. Phil. Trans. R. Soc. B Biol. Sci. 364(1526), 2013-2015. https://doi.org/10.1098/rstb.2008.0265

Hardesty, B.D., Harari, J., Isobe, A., Lebreton, L., Maximenko, N., Potemra, J., van Sebille, E., Vethaak, A.D., Wilcox, C., 2017. Using numerical model simulations to improve the understanding of micro-plastic distribution and pathways in the marine environment. Front. Mar. Sci. 4. https://doi.org/10.3389/fmars.2017.00030

Hidalgo-Ruz, V., Gutow, L., Thompson, R.C., Thiel, M., 2012. Microplastics in the marine environment: A review of the methods used for identification and quantification. Environ. Sci. Technol. 46, 3060–3075. https://doi.org/10.1021/es2031505

Hinata, H., Mori, K., Ohno, K., Miyao, Y., Kataoka, T., 2017. An estimation of the average residence times and onshore-offshore diffusivities of beached microplastics based on the population decay of tagged meso- and macrolitter. Mar. Pollut. Bull. 122, 17–26. https://doi.org/10.1016/j.marpolbul.2017.05.012

Isachenko, I., Khatmullina, L., Chubarenko, I., Stepanova, N., 2016. Settling velocity of marine microplastic particles: laboratory tests. Geophys. Res. Abstr. EGU Gen. Assem. 18, 2016–6553.

Isobe, A., Kako, S.I., Chang, P.H., Matsuno, T., 2009. Two-way particle-tracking model for specifying sources of drifting objects: Application to the East China Sea shelf. J. Atmos. Ocean. Technol. 26(8), 1672–1682. https://doi.org/10.1175/2009JTECHO643.1

Ivar do Sul, J.A., Costa, M.F., 2007. Marine debris review for Latin America and the wider Caribbean region: From the 1970s until now, and where do we go from here? Mar. Pollut. Bull. 54, 1087–1104. https://doi.org/10.1016/j.marpolbul.2007.05.004

Ivar Do Sul, J.A., Costa, M.F., 2014. The present and future of microplastic pollution in the marine environment. Environ. Pollut. 185, 352–364. https://doi.org/10.1016/j.envpol.2013.10.036

Iwasaki, S., Isobe, A., Kako, S., Uchida, K., Tokai, T., 2017. Fate of microplastics and mesoplastics carried by surface currents and wind waves: A numerical model approach in the Sea of Japan. Mar. Pollut. Bull. 121, 85–96. https://doi.org/10.1016/j.marpolbul.2017.05.057

Jahnke, A., Arp, H.P.H., Escher, B.I., Gewert, B., Gorokhova, E., Kühnel, D., Ogonowski, M., Potthoff, A., Rummel, C., Schmitt-Jansen, M., Toorman, E., MacLeod, M., 2017. Reducing uncertainty and confronting ignorance about the possible impacts of weathering plastic in the marine environment. Environ. Sci. Technol. Lett. 4(3), 85–90. https://doi.org/10.1021/acs.estlett.7b00008

Jalón-Rojas, I., Wang, X. H. and Fredj, E., 2019. Technical note: On the importance of a three-dimensional approach for modelling the transport of neustic microplastics, Ocean Sci. Discuss. https://doi:10.5194/os-2018-136.

Jambeck, J.R., Geyer, R., Wilcox, C., Siegler, T.R., Perryman, M., Andrady, A., Narayan, R., Law, K.L., 2015. Plastic waste inputs from land into the ocean. Science 347, 768–771. https://doi.org/10.1126/science.1260352

Jang, Y.C., Hong, S., Lee, J., Lee, M.J., Shim, W.J., 2014. Estimation of lost tourism revenue in Geoje Island from the 2011 marine debris pollution event in South Korea. Mar. Pollut. Bull. 81, 49–54. https://doi.org/10.1016/j.marpolbul.2014.02.021

Johnson, S.W., 1989. Deposition, fate, and characteristics of derelict trawl web on an Alaskan beach. Mar. Pollut. Bull. 20, 164-168. https://doi.org/10.1016/0025-326X(89)90486-4

Johnson, S.W., Eiler, J.H., 1999. Fate of radio-tagged trawl web on an Alaskan beach. Mar. Pollut. Bull. 38, 136–141. https://doi.org/10.1016/S0025-326X(98)00109-X

Kaiser, D., Kowalski, N., Waniek, J.J., 2017. Effects of biofouling on the sinking behavior of microplastics. Environ. Res. Lett. 12, 124003. https://doi.org/10.1088/1748-9326/aa8e8b

Kako, S., Isobe, A., Seino, S., Kojima, A., 2010. Inverse estimation of drifting-object outflows using actual observation data. J. Oceanogr. 66, 291–297. https://doi.org/10.1007/s10872-010-0025-9

Khatmullina, L., Isachenko, I., 2017. Settling velocity of microplastic particles of regular shapes. Mar. Pollut. Bull. 114, 871–880. https://doi.org/10.1016/j.marpolbul.2016.11.024

Koelmans, A.A., Bakir, A., Burton, G.A., Janssen, C.R., 2016. Microplastic as a vector for chemicals in the aqueEnvironment: Critical review and model-supported reinterpretation of empirical studies. Environ. Sci. Technol. 50(7) 3315–3326. https://doi.org/10.1021/acs.est.5b06069

Kooi, M., Van Nes, E.H., Scheffer, M., Koelmans, A.A., 2017. Ups and downs in the ocean: Effects of biofouling on vertical transport of microplastics. Environ. Sci. Technol. 51, 7963–7971. https://doi.org/10.1021/acs.est.6b04702

Lebreton, L.C.M., Greer, S.D., Borrero, J.C., 2012. Numerical modelling of floating debris in the world's oceans. Mar. Pollut. Bull. 64, 653–661. https://doi.org/10.1016/j.marpolbul.2011.10.027

Lange, M. and Van Sebille, E., 2017. Parcels v0.9: Prototyping a Lagrangian ocean analysis framework for the petascale age, Geosci. Model Dev., 10, 4175–4186. https://doi:10.5194/gmd-10-4175-2017

Liao, F., Wang, X.H., 2018. A study of low-frequency, wind-driven, coastal-trapped waves along the southeast coast of Australia. J. Phys. Oceanogr. 48, 301–316.

Ling, S.D., Sinclair, M., Levi, C.J., Reeves, S.E., Edgar, G.J., 2017. Ubiquity of microplastics in coastal seafloor sediments. Mar. Pollut. Bull. 121, 104–110. https://doi.org/10.1016/j.marpolbul.2017.05.038

Liu, Y., Weisberg, R.H., 2011. Evaluation of trajectory modeling in different dynamic regions using normalized cumulative Lagrangian separation. J. Geophys. Res. Ocean. 116, C09013. https://doi.org/10.1029/2010JC006837

Liu, Y., Weisberg, R.H., Vignudelli, S., Mitchum, G.T., 2014. Evaluation of altimetry-derived surface current products using Lagrangian drifter trajectories in the eastern Gulf of Mexico. J. Geophys. Res. Ocean. 119, 2827–2842. https://doi.org/10.1002/2013JC009710

Liubartseva, S., Coppini, G., Lecci, R., Clementi, E., 2018. Tracking plastics in the Mediterranean: 2D Lagrangian model. Mar. Pollut. Bull. 129, 151–162. https://doi.org/10.1016/j.marpolbul.2018.02.019

Liubartseva, S., Coppini, G., Lecci, R., Creti, S., 2016. Regional approach to modeling the transport of floating plastic debris in the Adriatic Sea. Mar. Pollut. Bull. 103, 115–127. https://doi.org/10.1016/j.marpolbul.2015.12.031

Lobelle, D., Cunliffe, M., 2011. Early microbial biofilm formation on marine plastic debris. Mar. Pollut. Bull. 62, 197–200. https://doi.org/10.1016/j.marpolbul.2010.10.013

Loeb, G.I., Neihof, R.A., 1975. Marine conditioning films, in: Advances in Chemistry, pp. 319–335. https://doi.org/10.1021/ba-1975-0145

Long, M., Moriceau, B., Gallinari, M., Lambert, C., Huvet, A., Raffray, J., Soudant, P., 2015. Interactions between microplastics and phytoplankton aggregates: Impact on their respective fates. Mar. Chem. 175, 39–46. https://doi.org/10.1016/j.marchem.2015.04.003

Macleod, A.K., Stanley, M.S., Day, J.G., Cook, E.J., 2016. Biofouling community composition across a range of environmental conditions and geographical locations suitable for floating marine renewable energy generation. Biofouling 32, 261–276. https://doi.org/10.1080/08927014.2015.1136822

Mansui, J., Molcard, A., Ourmières, Y., 2015. Modelling the transport and accumulation of floating marine debris in the Mediterranean basin. Mar. Pollut. Bull. 91, 249–257. https://doi.org/10.1016/j.marpolbul.2014.11.037

Martinez, E., Maamaatuaiahutapu, K., Taillandier, V., 2009. Floating marine debris surface drift: Convergence and accumulation toward the South Pacific subtropical gyre. Mar. Pollut. Bull. 58, 1347–1355. https://doi.org/10.1016/j.marpolbul.2009.04.022

Mellor, G.L., 1998. Users Guide for a Three-dimensional, Primitive-equation, Numerical Ocean Model, Program in Atmospheric and Oceanic Sciences, Princeton University.

Morét-Ferguson, S., Law, K.L., Proskurowski, G., Murphy, E.K., Peacock, E.E., Reddy, C.M., 2010. The size, mass, and composition of plastic debris in the western North Atlantic Ocean. Mar. Pollut. Bull. 60, 1873–1878. https://doi.org/10.1016/j.marpolbul.2010.07.020

Müller, R.J., Kleeberg, I., Deckwer, W.D., 2001. Biodegradation of polyesters containing aromatic constituents. J. Biotechnol. 86(2), 87-95. https://doi.org/10.1016/S0168-1656(00)00407-7

Murray, C.C., Maximenko, N., Lippiatt, S., 2018. The influx of marine debris from the Great Japan Tsunami of 2011 to North American shorelines. Mar. Pollut. Bull. 132, 26–32. https://doi.org/10.1016/j.marpolbul.2018.01.004

Neumann, D., Callies, U., Matthies, M., 2014. Marine litter ensemble transport simulations in the southern North Sea. Mar. Pollut. Bull. 86, 219–228. https://doi.org/10.1016/j.marpolbul.2014.07.016

PlasticsEurope, 2013. Plastics – the Facts 2013. Brussels, Belgium.

Röhrs, J., Christensen, K.H., Hole, L.R., Broström, G., Drivdal, M., Sundby, S., 2012. Observation-based evaluation of surface wave effects on currents and trajectory forecasts. Ocean Dyn. 62, 1519–1533. https://doi.org/10.1007/s10236-012-0576-y

Rummel, C.D., Jahnke, A., Gorokhova, E., Kühnel, D., Schmitt-Jansen, M., 2017. Impacts of biofilm formation on the fate and potential effects of microplastic in the aquatic environment. Environ. Sci. Technol. Lett. 4(7), 258-267. https://doi.org/10.1021/acs.estlett.7b00164

Sayol, J.M., Orfila, A., Simarro, G., Conti, D., Renault, L., Molcard, A., 2014. A Lagrangian model for tracking surface spills and SaR operations in the ocean. Environ. Model. Softw. 52, 74–82. https://doi.org/10.1016/j.envsoft.2013.10.013

Smith, S.D.A., 2012. Marine debris: A proximate threat to marine sustainability in Bootless Bay, Papua New Guinea. Mar. Pollut. Bull. 64, 1880–1883. https://doi.org/10.1016/j.marpolbul.2012.06.013

Sun, Y.J., Jalón-Rojas, I., Wang, X.H., Jiang, D., 2018. Coastal upwelling by wind-driven forcing in Jervis Bay, New South Wales: A numerical study for 2011. Estuar. Coast. Shelf Sci. 206, 101–115. https://doi.org/10.1016/j.ecss.2017.11.022

Talley, L.D., Pickard, G.L., Emery, W.J., Swift, J.H., 2011. Dynamical processes for descriptive ocean circulation, in: Descriptive Physical Oceanography, pp. 1–72. https://doi.org/10.1016/B978-0-7506-4552-2.10019-8

Thompson, R.C., 2004. Lost at Sea: Where is all the plastic? Science, 304, 838–838. https://doi.org/10.1126/science.1094559

Wakata, Y., Sugimori, Y., 1990. Lagrangian motions and global density distributions of floating matter in the ocean simulated using shipdrift data. J. Phys. Oceanogr. 20, 125–138. https://doi.org/10.1175/1520-0485(1990)020<0125:LMAGDD>2.0.CO;2

Wang, X.H., Symonds, G., 1999. Coastal embayment circulation due to atmospheric cooling. J. Geophys. Res. 104, 29801–29816. https://doi.org/10.1029/1999JC900183

Wang, X.H., 2001. A numerical study of sediment transport in a coastal embayment during winter storms. J. Coast. Res., ICS 2000 Proceedings, 414–427.

Weinstein, J.E., Crocker, B.K., Gray, A.D., 2016. From macroplastic to microplastic: Degradation of high-density polyethylene, polypropylene, and polystyrene in a salt marsh habitat. Environ. Toxicol. Chem. 35, 1632–1640. https://doi.org/10.1002/etc.3432

Ye, S., Andrady, A.L., 1991. Fouling of floating plastic debris under Biscayne Bay exposure conditions. Mar. Pollut. Bull. 22, 608–613. https://doi.org/10.1016/0025-326X(91)90249-R

Yoon, J.H., Kawano, S., Igawa, S., 2010. Modeling of marine litter drift and beaching in the Japan Sea. Mar. Pollut. Bull. 60, 448–463. https://doi.org/10.1016/j.marpolbul.2009.09.033

Zardus, J.D., Nedved, B.T., Huang, Y., Tran, C., Hadfield, M.G., 2008. Microbial biofilms facilitate adhesion in biofouling invertebrates. Biol. Bull. 214, 91–98. https://doi.org/214/1/91 [pii]

Zettler, E.R., Mincer, T.J., Amaral-Zettler, L.A., 2013. Life in the "plastisphere": Microbial communities on plastic marine debris. Environ. Sci. Technol. 47, 7137–7146. https://doi.org/10.1021/es401288x

Zhang, H., 2017. Transport of microplastics in coastal seas. Estuar. Coast. Shelf Sci. 197, 74–86. https://doi.org/10.1016/j.ecss.2017.09.032

Zhiyao, S., Tingting, W., Fumin, X., Ruijie, L., 2008. A simple formula for predicting settling velocity of sediment particles. Water Sci. Eng. 1, 37–43. https://doi.org/10.1016/S1674-2370(15)30017-X